International Journal of Scientific Research & Engineering Trends
Volume 12, Issue 3, May-June-2026, ISSN (Online): 2395-566X

Magnetic Material Characterization and Magnet Axis Displacement Measurement for Particle Accelerating

Sk Samsul Hoda, Professor Dr Vipin kumar
OPJS University

Abstract — Bending and focusing magnets, both normal- or super-conducting, are crucial elements for the performance of any particle accelerator. Their design require-ments are always more tighten regarding components' misalignment and mag-netic properties. This dissertation proposes new solutions for characterizing mag-netic materials and monitoring solenoids' magnetic axis misalignments. A superconducting permeameter is designed to characterize the new-generation superconducting magnet yokes at their operational temperature and saturation level. As proof of principle, the magnetic characterization of ARMCO®Pure Iron was performed at the cryogenic temperature of 4.2 K and a saturation level of nearly 3 T. A case study based on the new HL-LHC superconducting magnets quantifies the impact of the magnetic properties of the yoke on the performances of the superconducting magnets. A flux-metric based method is proposed to identify the relative magnetic perme-ability of weakly magnetic materials. As proof of principle, the magnetic prop-erties of the ITER TF coils quench detection stainless steel are analyzed. This method is not suitable to test materials with a relative permeability lower than 1.1. Hence, a measurement system based on a new magneto-metric method is conceived and validated employing a standard reference sample. The methods proposed in this thesis are currently employed at CERN's magnetic laboratory to face an increasing number of requests concerning not only the magnetic charac-terization of materials for magnets but also for shielding systems and compatibil-ity of various components with high magnetic fields. In this thesis, the results of the evaluation of ARMCO®Pure Iron as the yoke of the new LHC superconducting magnets and CRYOPHY as the magnetic shield for the cryomodule prototypes of HL-LHC Crab Cavities are reported. Finally, a new Hall-sensor method is conceived and implemented for monitor-ing the coils alignment in multi-coil magnets, directly during their operation in particle accelerators. The proposed method is suitable even for those cases when almost the whole magnet aperture is not accessible. Requiring only a few mea-surements of the magnetic field at fixed positions inside the magnet aperture, the method overcomes the main drawback of the other Hall sensor-based methods which is having to deal with sturdy mechanics of the moving stages. The method is validated numerically on a challenging case study related to the Solenoid B of the project ELI-NP.

Keywords— Instrumentation for particle accelerators, characterization of mag-netic materials, superconductivity and magnet protection, cryogenic measure-ments, superconducting magnets.

I. INTRODUCTION

Next-generation particle accelerators will produce a high number of collisions at very high energy, allowing the observation of new or rare phenomena of par-ticle physics. This will be made possible by increasing the "luminosity" and the"beam energy", the key performance parameters of an accelerator [67]. Inside the"European strategy for particle physics", major examples of these technological trends are the High Luminosity Large Hadron Collider (HL-LHC) and the High Energy LHC [81].

Precise and accurate measurement of the permeability, coercivity and resistivity of magnetic materials is of paramount importance to design and qualify acceler-ator magnets. A few national and private metrology laboratories offer this kind of measurements on the market. However, they typically have long lead times, limited capability to adapt to special needs and high cost. The MSC (Magnets, Su-perconductors and Cryostats) group at the European Center for Nuclear Research (CERN) is facing an increasing number of requests concerning not only the mag-netic characterization of materials for magnets, but also for shielding systems and compatibility of various components with high magnetic fields. Many of these applications stretch the envelope of test parameters beyond what is covered by international standards in terms of the range of values (accurate measurement of very low permeability), sample shape (such as wires, tapes or tubes, both in open and closed magnetic circuits) and volume (from a few grams of material to full-scale magnet yokes). Hence, an extensive upgrade of the instrument range of the CERN magnetic measurement laboratory has been necessary not only to adapt to these demands but also to face the campaigns of series tests as required by the High Luminosity upgrade of the Large Hadron Collider.

The CERN LHC is the world's largest and most powerful particle accelerator. The LHC consists of a 27-kilometer ring of

normal and superconducting magnets with a number of accelerating structures to boost the energy of the particles along the way. Inside the accelerator, two high-energy particle beams travel at close to the speed of light before they collide. The beams are guided around the acceler-ator ring by a strong magnetic field maintained by superconducting electromag-nets, that requires an operational temperature of 1.9 K. Thousands of magnets of different varieties and sizes are used to direct the beams around the accelerator. These include 1232 dipole magnets 15 m in length which bend the beams, and 392 quadrupole magnets, each 5–7 m long, which focus the beams. Just prior to the collision, another type of magnet is used to "squeeze" the particles closer together to increase the chances of collisions. Magnetic materials are important elements in the fabrication of magnets and take an important part in the overall accuracy. The selection of these materials and the development of measurement systems to support this selection have been considered carefully since the beginning of CERN.

The HL-LHC [31] is a project to upgrade the LHC to maintain scientific progress and exploit the LHC's full capacity [115]. By increasing its peak luminosity by a factor of five over nominal value, it will be possible to reach a higher level of integrated luminosity, nearly ten times the initial LHC design target. The HL-LHC will explore new beam configurations and new advanced technologies in the domain of superconductivity, cryogenics, rad-hard materials, electronics and remote handling.

Stronger superconducting dipole magnets will be installed in the dispersion

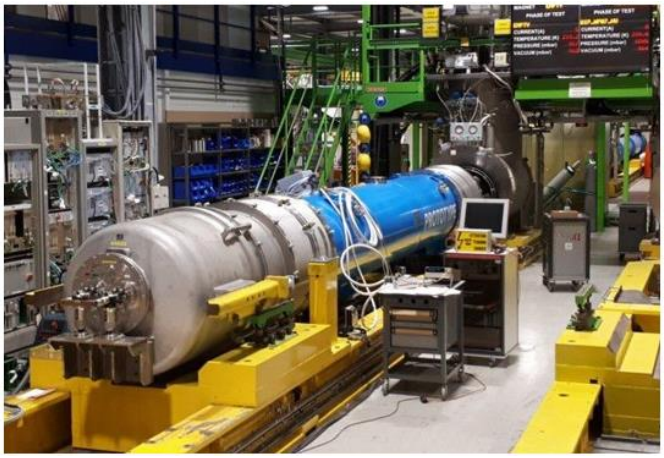

Figure 1: First Nb3Sn magnet on the CERN cryogenic test facility (SM18) horizontal bench

suppression zone to make space for additional collimators that protect the super-conducting magnets [134, 7]. The nominal magnetic field of the dipole magnets will increase from 8.6 T to 11.2 T. In Fig. 1.1 the first Nb3Sn magnet's test at the CERN cryogenic test facility (SM18) horizontal bench is shown. New supercon-ducting quadrupole magnets will be installed in the insertion region to increase the focusing properties of the machine, reaching the goal of a much higher lumi-nosity. The nominal field gradient of the new inner triplet quadrupole magnets will change from 200 T/m in an aperture of 70 mm to 132.6 T/m in an aperture of 150 mm [29]. In Fig. 1.2 the flux density in the cross-section of a 11 T dipole magnet for HL-LHC [122] and of the MQXF inner triplet quadruple are shown. In proximity of the coils, the iron yoke shows a level of flux density higher than T. This is due to the higher field generated in the aperture (11 T). The iron yoke

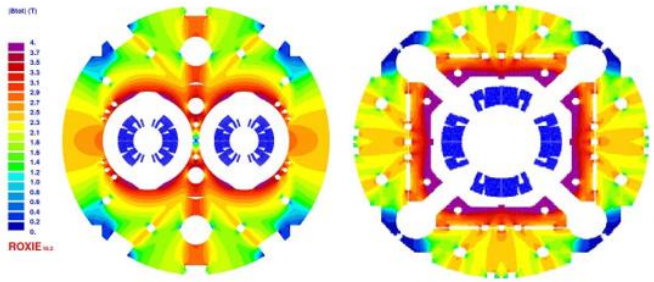

Figure 2: Flux density in the cross section of MBH 11 T dipoles (left) and in the MQXF quadrupole (right) for HL-LHC.

of a superconducting magnet is one of the key elements for its correct operation because it supplies the return path for the magnetic flux and, at the same time, gives mechanical rigidity to the cold mass.

In the past, low-carbon steel, known under the trade name MAGNETIL BLTM and produced by Cockerill Sambre-ARCELOR Group [61], was used for the pro-duction of the iron yoke laminations of the LHC main magnets. The magnetic characterization of this material is described in [20, 23]. This would have been the ideal choice also for the new HL-LHC magnets if it had still been available at the moment of the tender. Instead, ARMCO® Pure Iron Grade 4 produced by AK Steel has been chosen. 1800 tonnes of ARMCO®Pure Iron, to be used mainly for the single aperture Nb3Sn quadrupole magnets (inner triplet) MQXF [50] and 11 T Nb3Sn dipole magnets [122], needs to be firstly procured and then char-acterized magnetically to check that it satisfies certain requirements and quality

control standard. The HL-LHC magnet specifications prescribe 0.2 T at 1.5 T at 1200 A/m and 2 T at H = 24000 A/m. Considering the increasing level of flux density in these new magnets, see Fig.1.2, a characterization of ARMCO behavior for magnetic fields above 24 kA/m and at a temperature of 4.2 K is necessary to understand the behavior of the magnets at the new operating conditions.

The increase of luminosity will cause an increment of the radiation dose inside the accelerator. The magnets most affected by this higher level of radiation are the LHC Warm Bending Magnets (MBW) and Warm Quadrupole Magnets (MQW) [4]. Protection of these normal conducting magnets in the LHC aims to reduce the radiation dose received by the magnet's coils and increase their lifespan. This will be done by specially manufactured Tungsten Heavy Alloy (WHA) pieces [3]. The selected commercial material, INERMET® IT180 [110] contains 5% of nickel and copper in unspecified proportion and it is marketed as non-magnetic. However, according to the available literature, its magnetic properties depend critically on the precise composition. Even if slightly paramagnetic, an eventual residual mag-netization of this material could interfere with the magnetic field generated by the magnets and decrease the whole accelerator performance. Therefore, magnetic testing of the actually delivered pieces will be necessary. In particular, CERN has requested that the tungsten alloy used as radiation shield shows a relative mag-netic permeability, , lower than 1.005.

One of the main difficulties with accelerators is that the magnetic field that keeps particles in orbit must have the same configuration and intensity in all the dipoles. But when the magnets are on, a very strong force is produced, a force that can de-form the 'soft' parts of the magnets, such as superconducting coils. The force loading one meter of a dipole is about 400 tonnes (comparable with the weight of a Boeing 747), hence a huge deformation would occur without a mechanical com-ponent to keep the whole structure rigid. This component is the collar situated around the superconducting coils to prevent undesirable movements of the con-ductors. The collars must have well-defined geometry and physical properties to confine the coils, to avoid deformations, and have consistent behavior when ex-posed to extreme heat and magnetic fields. The problem has been solved using a particular alloy, belonging to the class of austenitic steels, that has all the proper-ties required: good thermal contraction and magnetic permeability. The material the collars are made of has to have a , lower than 1.003 to do not interfere with the flux density generated by the coil, as can be seen in Fig.

Hence, magnetic testing of the actually delivered pieces will be necessary also in this case.

Moreover, the High-Luminosity upgrade of the LHC will also exploit crabbing [133] for increasing and leveling the luminosity of the Large Hadron Collider (LHC). The idea is to deflect proton bunches so that their tilt at collision com-pensates for their crossing angle. This is achieved with bulk niobium supercon-ducting radio frequency (SRF) cavity cryomodules to be installed before the in-teraction points. Before Hi-Lumi definitive commissioning, one pair of these de-flecting (or crab) cavities has been successfully tested within a cryomodule with a proton beam in the Super Proton Synchrotron (SPS) at CERN in 2018 [31, 142]. Su-perconducting radio frequency (SRF) is considered as a promising technology in modern particle acceleration [46]. However, to guarantee optimum performance with a high quality factor, the initial magnetic field on RF surfaces of supercon-ducting cavities should be minimized [41], [90]. In fact, in cryomodules for the SRF cavity, magnetic shielding is a key technology [35]. Materials with a very high maximum relative permeability are used as passive magnetic shields: the magnetic flux is forced into the shielding material, and thus the magnetic field is canceled inside the shield, where SRF cavities are operating. The shield is some-times immersed in liquid helium at cryogenic temperatures, in order to be placed as close as possible to the SRF cavity. The cryogenic environment influences mag-netic properties, and special magnetic shielding materials have been designed for use in liquid helium [66], [63]. The initial magnetic properties, and therefore the performance of the magnetic shield, depend mostly on its composition as well as on the applied heat treatment. The magnetic shielding in the crab cavity cry-omodule is critical for achieving the operational stability required for HL-LHC. A solution with two layers of magnetic shielding consisting of a "warm" shield in the vacuum around the helium tanks, made of MuMetal, and a "cold" shield inside the helium tank directly around the cavity, made of Ni-Fe alloy Cryophy, has been developed for the SPS prototype cryomodule [133]. A magnetic sur-vey in the SPS concluded that an external field of no more than 200 T is to be expected during operation [22]. This estimate includes the effect of the earth's magnetic field and neighboring magnets. Hence, the magnetic shields were de- signed to ensure that no more than 1 μT reaches the cavity surface, with an ex-ternal field of 200T in the worst-case orientation [133]. The magnetic shield performance is strongly influenced by the material properties. Specifically, the design requirement for the cold shielding material is a relative magnetic perme-ability of minimum 105 at liquid helium temperature [5].

For the inner layer of the Crab Cavities' cryomodule, the Ni-Fe alloy Cryophy [1] has been used to reach optimum performance at cryogenic temperature [133]. Several works on magnetic shields and the related materials have been presented in literature, see Section 2.2.2. However, a magnetic characterization of the alloy Cryophy focused both on temperature and mechanical strain dependence, is not available [120]. Finally, accelerators performance is limited by "linear imperfections" induced by components misalignment and magnetic field errors. Therefore, the constraints on the position of the components for focusing, accelerating, or detecting the beam all along the accelerator must be increased and tightened [139]. These com-ponents are usually large and heavy, weighing often more than 100 kg and mea-suring several meters in length. They will have to be aligned to within a few of microns over a distance of several hundreds of meters. In the last decades, several methods have been developed to cope with the alignment of accelera-tor components [87, 95]. Of high importance is the alignment of focusing ele-ments, mainly quadrupole and solenoid magnets. While several methods have been developed and successfully applied to the alignment of quadrupole mag-nets [137], several problems arise from standard methods for solenoids [13, 12]. For instance, the single-stretched-wire method, a standard method for finding quadrupole magnets' magnetic axis, has much lower sensitivity when applied to solenoids, because the intercepted transversal field components are significant only at the magnet's ends [11]. When a magnet is in operation, its coils are con-stantly subject to an electrodynamic strain. The main reason resides in defor-mations caused by thermal effects, even with the installed cooling system. This could result in a significant misalignment of the magnetic axis from the geomet-ric axis. The thermal effects are especially present at the magnet start-up, but the misalignment can drift also during machine runnings, because of the heat gen-erated by particle beams.

Furthermore, when dealing with multi-coil solenoids, each coil may be affected by its peculiar misalignment. Hence, these misalign-ments have to be monitored when a strict constraint on the coils alignment is required, thus allowing to adjust the position of the coils to achieve/recover the solenoid design parameters. For instance, within the European project "ELI Nu-clear Physics" (ELI-NP) [47], this can be done with adjustable screws to translate and/or rotate a single coil, even during its operation. This system provides six degrees of freedom, and the desired position can be totally recovered on-line with a precision of tens of micrometers. Most of the standard methods for the solenoid axis identification are useless for on-line monitoring, owing to their need of ac-cessing a wide area of the solenoid's air gap (evidently, almost full of the beam-line and auxiliary accessories).

The research presented in this thesis proposes new solutions in the framework of magnetic material and axis displacement measurements for the challenges pre-sented in this chapter. The structure of the thesis is as follows

- Chapter 1: Introduction, where the problem statement that motivated this research is explained.
- Chapter 2: State of the art, where the content of the work is introduced. After a review of the principal materials for particle accelerator magnets, a literature overview of methods for characterizing magnetic materials and for measuring magnetic axis displacements is presented.
- Chapter 3: Proposal for characterizing soft magnetic materials, where the measuring principle of the flux-metric method and the enhancements car-ried out in this work, in terms of measurement procedure and drift correc-tion are illustrated. Firstly, the design aspects of the experimental support-ing technologies for data acquisition and analysis are described. Then, a solution for characterizing soft magnetic materials at the operational tem-perature of 4.2 K and at a saturation level near 3 T is proposed. The mea-surement system employs superconducting coils. Hence, specific quench detection and magnet protection simulations are carried out.
- Chapter 4: Proposal for characterizing weakly magnetic materials, where a flux-metric based and a magneto-metric methods are proposed for char-acterizing weakly magnetic materials with a permeability between 1.1 and 6.0 and lower than 1.005, respectively. The former method is an adapted-to-low-permeability-materials approach based on the standard flux-metric method for soft magnetic materials previously introduced. The latter is a novel method based on inverse analysis approach coupled with a finite-element model.
- Chapter 5: Proposal for monitoring magnetic axis misalignments , where a novel Hall transducers-based method is proposed for the on-line mon-itoring of solenoids' magnetic axis. In particular, the basic idea and the mathematical formulations of the method in the case of a single-coil and a multi-coil solenoid are presented.
- Chapter 6: Validation of the proposed method for soft magnetic materi-als , where the proposed measurement system based on the flux-metric ap-proach, are employed for characterizing two soft materials, namely, ARMCO for magnet yokes and CRIOPHY for magnetic shields. The importance of magnetic material measurements in the

framework of the design of mag-nets for particle accelerator is discussed, as well.

- Chapter 7: Validation of the methods for weakly magnetic materials, where the proposed flux-metric method is validated on a series production of co-wound

1.430 stainless steel tapes for the quench detection in ITER TF coils and the proposed magneto-metric based method is validated by using a reference alloy sample with a known relative magnetic permeability.
Chapter 8: Validation of the proposed magnetic axis monitoring method , where the proposed Hall sensors-based method for the real-time monitor-ing of single-coil and multi-coil solenoids is validated with a case study based on the requirements of the European project ELI-NP.
Chapter 9: Conclusions, where the conclusions and future perspectives are outlined.

II. STATE OF THE ART

This chapter summarizes the content of this PhD research. In particular, the most important materials for particle accelerator magnets are briefly reported and a literature overview of methods for their magnetic characterization is presented. Then, an overview of methods for measuring magnetic axis displacements are given. Finally, the objectives of this thesis are pointed out.

1. Materials for particle accelerator magnets

Magnetic materials are fundamental in satisfying the basic demands of our so-ciety, such as the generation, distribution, and conversion of electrical energy, the storage and retrieval of information, and even in media, telecommunications and biomedical applications. Nowadays, magnetic materials generate a market, whose value exceeds 1010 euros [52].

An in-depth treatment of magnetic materials goes well beyond the scope of this work. A general introduction to the magnetic properties of materials can be found in the text by Cullity an Graham [40]. The text by Bozorth [30] is a stan-dard reference, where an overview of the magnetic properties of different mate-rials can be found. Finally, the volume of O'Handley [34] and the comprehensive Handbook of Magnetism and Advanced Magnetic Materials [82] cover a number of advanced materials, including amorphous and nanocrystalline materials and advanced soft magnetic materials for power application.

This thesis is focused on the characterization of materials for particle accelerators. Before reviewing the measurement systems of magnetic materials mostly used in particle accelerators, it is necessary to survey those materials briefly. In particle accelerators, Iron-based alloys are widely employed for cores of accelerator and experiment magnets; Iron-nickel alloys are typically used as shields for the vac-uum chambers of accelerator injection and extraction septa; soft spinel ferrites are used in collimators to damp trapped modes; nanocrystalline materials are en-visaged for high-frequency transformers and amorphous materials for induction cores of heavy-ion inertial fusion-energy accelerators.

In particular, three categories have been distinguished and treated in this disser-tation:
i) materials for magnetic yokes, ii) materials for magnetic shielding and iii) weakly magnetic materials.

Soft magnetic materials for magnet yokes

Ferromagnetic materials are classifiable in two groups: Soft and hard magnetic materials. The difference between the two groups regards mainly the coercitive field, thus the current necessary to bring the magnetization of the sample to zero. As reported by Bozorth in [30], soft magnetic materials are defined as materi-als with high permeability and easy to be magnetized and demagnetized. Vice-versa, hard magnetic materials are defined as materials challenging to be mag-netized. This means that the difference between the two categories of material stays mainly in the value of coercitivity. For a soft magnetic material, the value of coercitivity is typically lower than 1000 A/m. The value of the peak permeability is typically higher or much higher than 1000 and the value of the initial relative permeability is typically greater than 500. These materials are commonly used for applications such as electrical machines or electro-magnets as iron yokes, to give the return path to the flux lines due to their high permeability. In order to minimize the hysteresis effects, the coercitivity of a material used in the core of an accelerator magnet is desired to be as small as possible. Usually, materials with coercivity smaller than 100 A/m are used. For a hard magnetic material, the value of coercitivity is much higher than 1000 A/m, with values of about 800 kA/m for NdFeB magnets and 3.3 MA/m for SmCo magnets. This property of conserving their magnetic state makes hard magnetic material suitable for the application of the magnetic memories. Moreover, because of the remanent field in the range of [0.8, 1.8] T, they are also used as excitation poles of the electrical motors.

Hard magnetic materials will not be treated in this thesis, where the focus will be given to soft magnetic materials. In particular, the properties of two groups of soft magnetic materials related to the fabrication of magnets' yoke and mag-netic shielding will be presented in the following paragraphs and next section, respectively.

Pure iron and low carbon steel for large accelerator DC magnet yokes

As reported by Sgobba in [124], a 'Pure iron' is an iron where the total concentra-tion of impurities (mainly C, N, O, P, S, Si and Al) does not exceed a few hundred ppm. An example of the impurities of a Pure Iron, ARMCO®from AK Steel, is given in Tab.2.1. Otherwise, it is preferably referred to as low-carbon steel. Very pure iron features a high electrical conductivity which makes it unsuitable for AC applications, due to the iron losses, its poor mechanical properties and its cost. When a few percentage of Si and Al are introduced in the alloy, it is usually referred to as "silicon steels". Fiorillo [52] reports several values for the magnetic properties of pure iron and low-carbon steels, shown in Tab.2.2. Generally, co-ercitivity values lower than 150 A/m and peak relative permeability significantly higher than 1000 are expected.

Saturation magnetization, depending only on the ferrite content in the lattice, is not influenced by the purity of the iron or by the operational temperature. Instead, impurities of the iron strongly influence coercitivity and relative per-meability. Values of initial and maximum permeability typically drop for cold worked material, whereas coercitivity increases. Annealing cycles allow to im-prove magnetic properties or restore them by reducing internal strains, increas-ing the grain size and allowing better diffusion of the impurities. Two are the classes of anneals used commercially: Anneals below 900◦C and anneals at or about 925◦C or higher to promote grain growth. These anneals should be fol-lowed by slow cool. For further details about metallurgy and annealing pro-cesses, reference is made to the dedicated literature [60].

Materials for particle accelerator magnets

Composition	Max. Analysis %
Carbon (C)	0.005
Manganese (Mn)	0.060
Phosphorus (P)	0.005
Sulfur (S)	0.003
Nitrogen (N)	0.005
Aluminum (Al)	0.005
Nickel (Ni)	0.03
Chromium (Cr)	0.03

Impurities composition in ARMCO®Pure Iron Grade 4. [source: AK steel datasheet]

TABLE 2: Typical values of the magnetic parameters of soft magnetic materials. [52]

Material	H_c [A/m]	μ_{ri}	μ_{rp}
Ingot (99.8% Fe)	112	10	1000
ARMCO	80	200	7000
Commercially pure	20-100	200-500	3500-20000
Carbonyl iron powder		6	3000 20000
Vacuum-melted	25 -	21000	
Electrolytic		7	1000 26000
Electrolytic annealed	18 -	41500	
Vacuum-smelted and hydrogen-annealed	3	-	88400
Purified ARMCO (99.5% Fe)		4	10000 227000
Vacuum-annealed	-	14000	280000
Single-crystal	-	-	680000
Single-crystal, magnetically annealed	12	-	1430000

Low-carbon steel for LHC magnets yokes

For applications that require good magnetic properties but at a reasonable cost, low-carbon steels are frequently used. As reported by Fiorillo in [52], low-carbon steels for magnetic cores are generally produced as sheets, through a sequence of hot and cold rolling and thermal treatments. In order to improve the magnetic properties, the laminations are often decarburized. Performance of low-carbon steels is described typically as AC magnetic properties at industrial range fre-quencies. In the absence of any purification treatments and high considerable silicon content, AC losses at 60 Hz and 1.5 T can reach 15 W/kg, with a relative permeability of The addition of roughly 1% of silicon com-bined with a proper composition control allows reducing power loss to 8 W/kg with a relative permeability of roughly 2000. Typically, they are delivered in lam-inations with a final thickness of 0.50-0.85 mm. Contrary to high-purity irons, low-carbon steels are affected by magnetic aging, where for aging it is intended an increase of the coercivity that occurs with time, due to the formation of cemen-tite precipitates that give rise to domain wall pinning. Cementite is a phase of the steel where carbon is deposited on the boundary of the grains: since carbon is a diamagnetic material, this creates a domain wall pinning. Generally, pure iron and non-alloyed steels are mostly used for DC and quasi-DC magnets for their low-cost and because power losses are not considered.

Iron-silicon alloys for steering and corrector magnet yokes

The addition of few percents of silicon to a decarburized low-carbon steel changes the iron properties considerably. Silicon steels are classifiable in two groups: non-oriented and grain-oriented silicon steels. Non-oriented silicon steels are soft magnetic materials with isotropic grain texture, which covers the applica-tions of the electrical rotating machines, where the isotropy of the material is strongly recommended. Grain-oriented silicon steels, differently from the non-grain oriented, exhibits a preferential direction of magnetization: this means that they are anisotropic and have minimum coercitivity and maximum permeabil-ity when magnetized in their preferential direction. The application of grain-oriented steels is restricted to most of the transformers cores, where it is nec-essary to have

the best performances along the rolling direction, that gives the return path to the magnetic flux. A first advantage is that the electrical resistivity increases at a rate of 5x10−8 Ωm per soluted atomic percent, improving in this way the material performance in AC for the power losses. Other advantages of Silicon-iron alloys are availability, punchability, precisely defined characteristic, and low coercitivity value, an essential feature for the linearity of magnets work-ing with variating fields of either polarity. As a drawback, it is possible to register a reduction of the saturation magnetization (from 1.6 T of low-carbon steels to 1.4-1.5 T) and higher costs. This is the reason why low carbon steels are preferred for large-scale magnet yokes, while silicon-iron are used for small magnet yokes such as steering and corrector magnet yokes.

Soft magnetic materials for magnetic shielding

Magnetic shielding is of paramount importance for guaranteeing good perfor-mance of cryomodules in particle accelerators. The effect of stray magnetic fields on the quality factor(Q0 of the superconducting radio frequency (SRF) cavity is regulated by the following equation [119]: Q , where G is the geometric

Materials for particle accelerator magnets

factor of the cavity and Rs is the cavity resistance. The latter can be divided into two contributions, namely the surface magnetic field (RH) and other com-ponents. The RH is directly proportional to the external magnetic field that, in case we consider only the earth's magnetic field, is roughly 50 µT. Hence, a high stray magnetic field increases the cavity surface resistance, causing a degradation of the cavity's quality factor. The standard way to prevent this is by employing magnetic shields [99]. Two classes of magnetic shields are generally employed, namely active shield [27] and passive shield [86]. The former is based on the use of a superconducting coil to generate a magnetic field that cancels out an eventual external magnetic field. The latter that provides a path for the field lines around the shielding volume, and minimizes the magnetic field inside the cryomodules, by drawing the field onto itself.

Materials with a very high maximum relative permeability are used as passive magnetic shields. The shield is sometimes immersed in liquid helium at cryo-genic temperatures. The magnetic shielding in the HL-LHC crab cavity cryomod-ule is made of CRIOPHY. A registered trademark of Aperam, CRIOPHY is a Ni-based ferromagnetic alloy, namely 81% of Fe, 14% of Ni, and 5% of Mo in weight. It is specifically aimed to maximize magnetic permeability at cryogenic temper-atures, by a tailored composition and a defined heat treatment. Cryophy is very similar in most properties to MuMetal (ASTM A753, alloy 4), which is used as the 'warm' magnetic shielding of the crab cavities outside of the helium tank. In general, Nickel-iron alloys present a wide range of behaviors depending on the percentage of nickel, in the range from the 35% to 80%. The percentage of nickel is what influences mostly the magnetic properties, giving an extensive range of possible application for such materials. For example, at a concentration of 36% it is possible to observe a significant drop of the Curie temperature which reaches a value of 230 °C, which increases the resistivity (75x10−8 Ωm) and makes the ma-terial performant at high frequencies. An alloy with this nickel content is mostly used for radar pulse transformers (Fe64-Ni36). By increasing the content of nickel at a value of 50% (Fe50-Ni50), the saturation polarization is of 1.6 T. Using ther-mal treatments [52], it is possible to achieve a squared hysteresis cycle, compatible with the application of magnetic amplifiers. With a content of nickel that keeps increasing, at a value of 55-60%, by annealing under a transverse saturation field, it is possible to achieve a remanent flux density of 0.9-1.2 T, compatible with the use of unipolar pulse transformers (power electronics devices) or ground fault in-terrupters. The highest permeabilities and lowest coercitivities are achieved with a content of nickel of 75-80%, where with the addition of elements like copper or chrome, it is possible to increase the resistivity of a factor 3 or 4, have a coercive field lower than 1 A/m and initial relative permeabilities higher than 100000. These kinds of alloys are known as supermalloys and their use is adopted for magnetic shielding applications. As a drawback, these alloys are all susceptible to heat treatments and the degree of cold working. Moreover, a heat treatment atnvery high temperatures (1100◦C) is always recommended after shaping.

Weakly magnetic materials

Weakly magnetic materials are materials with relative magnetic permeability in the range µr = 1.00001 to 6. In science and industry, several technological issues arise where structural materials and components with vanishing (ideally zero) magnetic behavior are required. In practical alloys, such as austenitic steels, brass and bronze, traces of magnetism are present as a rule [53]. Non- magnetic mate-rials are an issue for the design of particle accelerator equipment. Among metals, aluminum is undoubtedly the standard used, although its strength and elastic modulus are often too low for specific applications. Titanium has a better be-havior in this sense, but it is used mainly in special vacuum chambers, because of its reduced availability and high costs. Ceramics are even better in many as-pects, but even more expensive and brittle than the other materials listed above. Considering their high mechanical strength, stainless steels are the ideal choice as structural elements of particle accelerator components, but attention has to be paid to quality control of the vanishing magnetic properties.

Structural materials for fusion magnets
Austenitic stainless steels are widely used in hostile environments, such as nu-clear reactors, naval vessels, and chemical plants, where the combination of good corrosion resistance with high strength, stiffness, and toughness is required. How-ever, the metastable austenitic (γ) phase is easily transformed into ϵ or/and α′martensitic phase, owing to the deformation during manufacturing or fatigue during service. With an increase of martensitic transformation, the strength of the material increases, while ductility and corrosion resistance decreases.

Industrial specifications typically call for an upper limit of the magnetic suscep-tibility of these materials, ranging from a few units to some 10−3 , and practical methods to characterize faint susceptibility material are therefore needed. As an example, in the framework of quench detection in ITER Toroidal coils (TF), considering the strong field predicted, co-wound stainless steel tapes with a rel-ative permeability lower than two must be used. Nevertheless, during produc-tion, these steel tapes are subjected to different levels of mechanical and ther-mal stresses [143]. In practice, after the manufacturing process, the magnetic and paramagnetic material properties are changed. Consequently, the measurement of the actual magnetic properties of the material is needed.

Stainless steel for collars of superconducting magnets
Superconducting magnets' coils are subjected to a strong force proportional to the flux density generated by the magnet itself. Generally, the coils are held in place by using stain steel holders, called 'collars'. The material the collars are made of has to have a μr, lower than 1.003 to do not interfere with the flux density generated by the coil, as it can be seen in Fig. 1.2. Hence, magnetic testing of the actual delivered pieces is critical.

For the collars of the new LHC superconducting magnets, the structural material chosen is an austenitic steel P506 produced by Voestalpine supplier. P506 is a

Materials for particle accelerator magnets
stainless steel specially developed by CERN belonging to the family of high Mn, high N stainless steels [126]. This special composition (approx. 0.012%C, 19%Cr, 11%Ni, 12%Mn, 0.9%Mo, 0.3%N) allows low relative magnetic permeability to be maintained down to cryogenic temperatures.

Tungsten-based alloys for coils' radiation protection
In the upcoming LHC upgrade at CERN, higher luminosity will boost the radi-ation dose received by the accelerator magnet's coil and consequently decrease its lifespan, as assessed in Chapter 2. Hence, a radiation shield with relative permeability less than 1.005 is required for some of the magnets closest to the detectors. The selected commercial material, INERMET® IT180 [110] contains 5% of nickel and copper in unspecified proportions and it is marketed as non-magnetic. However, according to the available literature, its magnetic properties depend critically on the precise composition. Even if slightly paramagnetic, an eventual residual magnetization of this material could interfere with the magnetic field generated by the magnets and decrease the whole accelerator performance. Tungsten composites are metal-metal composites produced by liquid phase sin-tering of mixed tungsten (90-97 %), nickel, iron, copper, molybdenum and cobalt powders. After proper sintering, the material consists of spherical tungsten par-ticles embedded into a solid solution Ni-Fe-W(Co), Ni-Fe-W(Mo) or Ni-Cu-W matrix. These composites exhibit a unique combination of high density (17-18.6 g/cm3), high strength (700-900 MPa), excellent corrosion resistance, dumping capability, good thermal and electric conductivity and relatively high ductility, which allow them to withstand moderate amounts of cold working. Their prop-erties make them attractive for many applications: balance weights, welding elec-trodes, extruding dies, anti-vibration holders for tools penetrators. The ductility and strength of tungsten composites strongly depend on their microstructure, which in turn is controlled by thermal treatment and trace impurity content. Tungsten composites are increasingly used worldwide as radiation shields. They successfully replace lead, formerly used for this application. The advantage of tungsten composites over lead is the combination of radiographic density, machin-ability, good corrosion resistance, high radiation absorption, high strength, high melting temperature and, what is always emphasized, lack of toxicity [10]. Pro-tection of the normal conducting magnets MQW and MBW in the LHC will be done by specially manufactured, non-magnetic Tungsten Heavy Alloy (WHA) pieces. These pieces shall comply with ASTM B-777 class 3 with the iron content, which has to be below 30 ppm. This yields the following material composition: density > 18g/cm3; yield strength > 600 MPa; tensile strength > 650 MPa; elon-gation at breakage > 1%.

2. Characterization of magnetic materials
The characterization of magnetic materials is of paramount importance not only during the electromagnetic design of magnets but also during the magnet's pro-duction for guaranteeing good quality control, especially for large-scale produc-tions. In electromagnetic design, the knowledge of how a certain material replies to a certain applied field (normal magnetization curve) is essential. it depends on several factors, such as the quantum phenomenology at the atomic level and the composition of the lattice, that give rise to a resultant

macroscopic effect of the response. The magnetic behavior of a material is also strongly influenced by the lattice content. In this thesis, it will be shown how the impurity content influ-ences the property of pure iron or the percentage of nickel deeply influences the properties of an iron-nickel alloy, thus its destination of use.

On the other side, magnetic measurements of materials are, also, needed to en-sure quality control during magnets' production. For example, magnets in par-ticle accelerators are usually powered in series. What is essential for particle ac-celerator is that all the magnets behave the same. Hence, an excellent level of reproducibility of their magnetic behavior has to be guaranteed.

The magnetic characterization of materials can be directed both at the measure-ment of intrinsic properties, such as saturation magnetization, magnetic anisotropy and Curie temperature and at the determination of magnetic constitutive law, as embodied by the magnetization curves and the related hysteresis phenomena [52]. In this thesis, we will concentrate on the latter point and the related measur-ing techniques. Several methods and standards have been developed for mea-suring materials' magnetic properties. These methods depend on many different parameters, such as:

- Waveform and frequency of the excitation current: sinusoidal excitation (AC) at low, medium and high frequency or quasi-static excitation (DC) as described in the IEC 60404 series [38, 39, 70].
- Expected relative magnetic permeability of the material under test ($\mu r \approx 1$, μr = 103- 104 , μr >105).
- Sample shape (rings, laminations, needles, cylinders) and size.
- Portability of the instrumentation.
- Anisotropy of the material.
- Temperature at which the measurement is performed (cryogenic, room tem-perature, high temperatures).

A classification based on the specific physical effect exploited in revealing the magnetic state of the material is found in [53]: (i) Force techniques; (ii) Flux-metric techniques; (iii) Magneto-metric techniques; (iv) Magneto-optical techniques; (v) Magneto-strictive techniques; (vi) Magnetic resonance methods. This thesis's re-search will focus on the flux-metric and magneto-metric measuring methods. In

Characterization of magnetic materials

the former, a coil linked with the test sample is the location of an electromotive force following a change in the material magnetization engendered by the ap-plication of a magnetic field. The magnetization is determined by integrating the induced voltage. In the latter, the field lines emitted by an open sample are intercepted and related to the magnetization of the material. In the following three paragraphs an overview of the methods to characterize the three categories of magnetic materials previously distinguished (weakly magnetic materials, soft magnetic materials, and materials for magnetic shielding) is given.

Characterization of materials for magnet yokes

The characterization of soft magnetic materials is a very vast subject. The most re-cent book covering this field was written by Tumanski [136]. Collecting state-of-the-art knowledge from information scattered throughout the literature, Hand-book of Magnetic Measurements describes magnetic materials and sensors, the testing of magnetic materials, and applications of magnetic measurements. In the text by Fiorillo [52] a review of the most important methods is presented as well. Several methods to characterize soft magnetic materials at several frequencies are presented, as well. These methods are essential in applications, such as trans-formers, generators, motors and for electric power generation, where the core loss in Watt/kg is the most critical parameter. On the contrary, in particle accel-erator magnets, soft magnetic materials are mainly used as electromagnet yokes, where magnetic fields are fixed or slowly varying and core loss is no longer the important parameter. The rate of change of the induction in the gap of a particle accelerator magnet is in the order of 10 T/s. Therefore, quasi-static measurements (DC) provide the best estimate of material magnetic properties. In this section, the three main commonly used techniques to measure soft magnetic materials with consideration to the application of particle accelerator magnet core, namely ring method, Epstein frame and single sheet tester, are introduced. A particular focus is given to the instruments, based on these three techniques, developed at CERN magnetic laboratory. All the three hereafter described methods and apparatus follow the same flux- metric and close-loop principle and are based on the mea-surement of a transient voltage induced on a secondary winding by a step-like field variation applied on a primary winding.

Epstein frame

The Epstein frame is one of the most used standards for measuring the global magnetic properties of electrical steels. The IEC standard 60404-2 'Epstein frame'applies to non-oriented and grain-oriented sheets and strips for DC and AC mea-surements at frequencies up to 400 Hz [71]. The Epstein frame is a sort of un-loaded transformer. It consists of a non-magnetic square form, where four sets of primary and secondary windings are wound. The sample consists of steel strips placed inside the non-magnetic square form in a way that a closed magnetic path is formed. The main advantages of this

method are the wide ranges of magnetiza-tion frequencies (0-100 kHz) and magnetic field intensities (0.2 A/m - 10 kA/m); the good accuracy of the results and the easy machining of the samples. The main drawbacks are the inhomogeneity of the magnetic circuit due to the overlapping corners and the definition of a mean path length, even though it varies with the peak flux density, excitation frequency, permeability and anisotropy of the mate-rial under test.

At CERN the Epstein frame has a somewhat limited application, while in the in-dustry it is a standard for AC measurements (50 Hz losses). On the other side, it overcomes the ring method's problem of measuring anisotropy of magnetic materials. An adapted-to-CERN-needs version of the Epstein frame has been de-veloped to measure thinner steel laminations than the standard Epstein frame. This makes the production of the sample quite easy, requiring just a simple cut-ting of the lamination. An Epstein frame can be used as a permeameter at the exception of the saturation where it is less and less precise due to the increasing flux leaks at the corners [24].

Single sheet tester

The single sheet tester is another standard method to measure the magnetic prop-erties of electric sheets, as reported in the standard IEC 60404- Part 3: Methods of measurement of the magnetic properties of electrical steel strip and sheet utilizing a single sheet tester [37]. It is mainly designed for fast measures of the coercitivity Hc of the material under test. In [62] a compensated Single Sheet tester was devel-oped to measure very soft materials with high precision. The main advantages of SST are that the excitation field can be limited to 1200 A/m. Considering that Hc is maximum at 1.5 T, it is possible to measure anisotropy. Generally, there is no sample preparation and measurements are very fast (a few minutes). The main disadvantages are the difficulty to guarantee a good contact between the sample and the yokes to minimize a parasitic air gap; the relative magnetic permeability in the yoke material must be considerably higher than in the sample, this limits the use of this method to the measure of iron-based alloy; accurate positioning is needed to avoid displacement of the yokes with respect to each other. In accel-erators, a crucial parameter is the reproducibility between magnets of the same kind. Considering that magnets are powered in series, the main sources of dif-ferences between them are the mechanical accuracy and the magnetic properties of the yokes. In order to guarantee a good level of yoke to yoke reproducibil-ity, a good quality control, of the coercitivity and the relative permeability of the material used for the production, is essential. Considering the good correlation exciting between these two parameters, a whole production can be sufficiently well controlled by an SST, saving costs and time. The Ring method can be used as a reference.

This is the reason why at CERN a customized version of the single-sheet tester, called coercimeter [25], has been designed and used for decades to characterize tons of steel laminations for magnet yokes of several large-scale projects, such as the Large Electron-Positron (LEP) collider (11000 tons) and the LHC (50000 tons). In particular, the coercimeter was designed to measure steel sheets with-out preparation and just before being punched. It uses a Mumetal yoke material

Characterization of magnetic materials

in order to guarantee a good flux return with minimum coercitivity. Nowadays, the main hardware components are still available. However, the interface and control software and several electronic components are obsolete.

Ring method

A series of standards, denoted by IEC 60404, groups basic magnetic measure-ments in electrical steels. In particular, in the standard IEC 60404- Part 4: Methods of measurement of d.c. magnetic properties of iron and steel [72] the ring method is presented. A detailed discussion of this method will be given in chapter 3. Here the main advantages and drawbacks are highlighted. Any air gap, ends or dis-continuity in a magnetic circuit create a demagnetizing field, which opposes the applied field and reduces the induction level in the material under test. The main advantage of ring samples is that they are free from demagnetizing fields. On the contrary, the excitation field inside the sample is not constant and varies with the inverse of the radius. A ring sample is not too difficult to machine even if atten-tion has to be paid to avoid heating or surface cold working during machining. A drawback is that with a ring method is not possible to take into account any anisotropy in the material, because, unlike the single sheet tester, it only gives an averaged value. With a ring method, the coercimeter value can be easily un-derestimated. If a sample is made of several laminations, with a relatively large anisotropy, stacked on each other, a sort of magnetic short-circuit could occur and generate a significant error on the coercitivity measure. The main disadvantage of this method is having to install new windings for each new sample, which can be quite a long and tedious work.

At CERN, this problem has been overcome by designing and developing the'split-coil' permeameter [65], where the coils have been split into two halves. Good quality interconnections have been used considering the number of con-nection (two per turn all in series). The main advantage of this solution is the significant reduction of the measurement duration, allowing the

use of this de-vice for the quality control of large productions. On the other hand, a drawback is that the heat dissipation limits the maximum excitation field to 24000 A/m for some seconds, preventing the study of the saturation region.

Magnetic properties of materials at high fields

In this thesis, a distinction between the characterization at standard fields and high fields is made. Where standard fields mean a magnetic field lower than about 24000 A/m (approximately the magnetic field needed to bring the material in saturation).

Characterization at this field values is particularly required for normal-conducting magnets. Even though the characterization at standard fields allows to obtain the value of saturation magnetization, characterizing a ferromagnetic material at higher fields is essential for superconducting magnets: Typically the initial mag-netization curves are delivered up to a field value of roughly 48 kA/m. Data for higher field values are extrapolated using empirical models and fitting algo-rithms. Characterization of magnetic materials at high fields allows these models to be improved or validated.

A similar problem of characterizing the magnetic properties of a material for such a wide range of fields was described in [78] for the 10 T single and twin aper-ture dipoles developed at the National Laboratory for High Energy Physics in Japan (KEK) in collaboration with CERN. Moreover, a similar characterization was done for the iron yoke of the LHC magnets, reaching a magnetic field up to 2.5 T [20, 23].

Characterization of materials for magnetic shields

The methods presented in the previous section are also employed for character-izing magnetic shielding materials such as MuMetal and CRIOPHY, but the mea-surements are typically performed at very low fields. This because a magnetic field H of 10 A/m is already enough to bring these materials in saturation. In this section, the focus is given to characterizations and magnetic shielding appli-cations of such materials, rather than on the method itself used.

Several interesting research works on magnetic shield have been presented in lit-erature [135]– [94]– [56]– [6]. In [135], magnetic properties and shielding charac-teristics of multilayered Ni80Fe20/Cu film shields were investigated as a function of thickness and number of layers. Moreover, the main shielding mechanisms for multilayered Ni80Fe20/Cu film samples under different external influences were discussed. In [94], an experimental research on the magnetostatic shielding effec-tiveness of a single-layer cylindrical sample of the shields based on electrolyti-cally deposited Ni80Fe20 alloy was carried out. It has been shown that in the magnetic fields range from 100 A/m up to 2700 A/m, the shields based on the Ni80Fe20 alloy are preferred over ones based on the 84KHSR amorphous ribbon. Several further works specifically focused on the characterization of magnetic shield materials, have been presented [43]–[97]. In [43], first the effect of the mag-netic field on the gain and charge collection of some large-aperture photomulti-plier tubes were investigated. Then, the photomultiplier magnetic shield, made of the material FINEMET, was described. In the presence of the Earth's magnetic field, this type of shielding was proved capable of significantly increasing the col-lection efficiency of photoelectrons, as well as improving the response uniformity of these tubes.

In [120], the magnetic properties of two important passive magnetic shielding materials (A4K and AMuMetal) for accelerator applications, subject to various processing and heat treatment conditions, were studied over a wide temperature range. The effect of processing on the degradation of the magnetic properties of both materials was also investigated. The authors state that while some prior work exists on characterizing the magnetic properties of such materials, a com-prehensive study of the effect of deformation during the manufacturing process and annealing on the magnetic permeability of shielding materials over a broad range of temperatures (from cryogenic to room temperature) is still not available in the literature. Their paper bridges this gap by performing such experimental studies, yet only for A4K and AMuMetal samples.

Characterization of magnetic materials

In [98], the magnetic properties of Cryophy, the material of interest for CERN crab cavity cryomodules [133], were measured at room and cryogenic temperatures Furthermore, the permeability dependence on the maximum annealing temper-ature (1100◦ and 1170◦ C) was examined on ring samples. From these data, Cryophy was chosen as the magnetic shielding material for the superconducting cavities in the main linac section of the compact Energy Recovery Linac (cERL) at the High Energy Accelerator Research Organization (KEK), in Japan. The effect of mechanical deformation on the magnetic permeability of magnetic shields is investigated in [97], where a significant degradation of the magnetic permeabil-ity with mechanical strain was observed on high Ni-content alloys. However, their exact composition was not disclosed. Furthermore, although the magnetic properties are measured at room and cryogenic temperatures, the permeability dependence on the heat treatment conditions is studied in view of a specific ap-plication target for ERL. Analyzing the results and conclusions in these papers, it is evident that:

- the requirements of the magnetic shield on the Cryophy magnetic perme-ability is challenging and requires experimental studies on samples of the same material used for the cryomodule;
- few magnetic characterizations of high Ni-content alloys are presented in literature, including Cryophy;
- a comprehensive magnetic characterization of this alloy, focused both on temperature and mechanical strain dependence, is not yet present in litera-ture;
- moreover, as stressed in an inter-laboratory study on the precision and accu-racy of determining the soft magnetic properties of high-permeability ma-terials utilizing direct current (DC) methods, the repeatability and repro-ducibility of the results are low [129].

Characterization of weakly magnetic materials

In this section, an overview of the main methods to measure the relative perme-ability of weakly magnetic materials is presented. A special focus is given to the methods developed at CERN magnetic laboratory.

The ASTM international standard A342/A342M-2014 [18] describes four proce-dures for the determination of relative permeability of materials having a perme-ability below 6.0: Test method I - Fluxmetric method; Test method 3 - Low mu permeability indicator; Test method 4 - Flux distortion and Test method 5 - Vi-brating sample magnetometry.

In the previous editions of the standard a test method number 2, called "Per-meability of paramagnetic materials", was also included. However, in the last edition, it was eliminated as an acceptable method of testing. Nevertheless, in recent literature, a relevant number of authors still refer to this method, and so it has also been included in this overview.

Fluxmetric Method - Test method I

This method allows permeability between 1.0 and 4.0 to be measured. Usually, it is used for design purpose, specification acceptance, manufacturing control and R&D. The classic layout of the method is illustrated in Fig. 2.1. The main components are a source of DC current; a magnetizing solenoid with a pair of test coils, one for measuring magnetic flux density and the other for compensating the air flux; and a fluxmeter for measuring the magnetic induction. The test specimens can have the shape of a bar, rod, wire, or strip with a uniform cross-section.

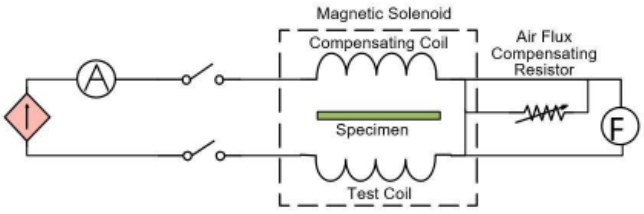

FIGURE 2.1: Example of fluxmetric measurement system layout. Adapted from [18]

It allows the selection of the magnetic field at which the permeability is measured by adjusting of the DC power supply. The use of compensating coils causes an increase of the method's accuracy. However, because of the specimen shape, a demagnetization field will be generated. This leads to an overestimation of the magnetic field strength and a reduction of the flux leakages in the B-coil.

Permeability of paramagnetic materials - Test method II

Even if excluded from the ASTM standard, an alternative to the flux metric ap-proach is represented by a group of methods called "Force methods". These meth-ods have high accuracy when dealing with permeability close to unit. The most common are the Faraday balance and the Gouy technique [114], [144]. These methods are suitable for measurement of materials with $\mu < 1.05$.

A general layout of the measurement system is depicted in Fig. 2.2.

Characterization of magnetic materials

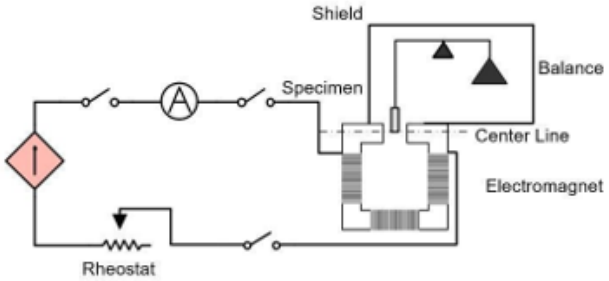

FIGURE 2.2: Classic layout of a force method measurement system.

Adapted from [18].

After demagnetizing the sample and calculating its cross-sectional area, the spec-imen is suspended from the balance. A magnetizing current is turned on and set to such a value as to give a magnetic field strength of 80 kA/m, minimum. The permeability is calculated from the apparent change in mass of the specimen. Force methods can display better sensitivity than

flux metric methods, but they are rather cumbersome and time-consuming. Because of restrictions on the spec-imen shape (typically very small), these test methods are most often used to eval-uate semifinished products before are manufactured.
At CERN, a built-in magnetic balance has been used for decades to measure weakly magnetic materials before and during the production of several com-ponents later installed in the LHC and several other CERN experiments [125]. Nowadays, the main hardware components are still available. However, the in-terface and control software and several electronic components are obsolete.

Low-μ permeability indicator - Test method III
The low-μ permeability indicator is based on comparing the permeability of a tested specimen with a standard insert, with known permeability [57]. Hence, it provides test values suitable for specification purpose, generally stated as "per-meability is less than". Usually, these instruments are portable, commercially available and present the advantage of being able to test specimens of all forms and shapes, providing that there is a suitable flat surface [88]. A drawback of these instruments is that usually the measurements are made in a magnetic field strength of only 8 kA/m, where a magnetic field of roughly 80 kA/m is generally recommended.

Flux Distortion - Test method IV
Instruments based on other methods, for example, flux distortion, such as the Fo-erster Magnetoscop [73], are also commercially available. The method, schemat-ically shown in Fig. 2.3, is suitable for materials with relative permeability be-tween 1.0 and 2.0.

The permeability measuring method is based on the fact, that every permanent magnet possesses a defined distribution of lines of force. All lines of force of a cylindrical permanent magnet run in a plane through the center of the cylinder between the two poles that are parallel to the cylinder axis. A gradient probe is placed on either side of the cylindrical magnet in this plane perpendicular to the cylinder axis at the center of the permanent magnet. The lines of force of the magnet are perpendicular to the axis of the two probes. Therefore, they do not measure the magnetic field of the cylindrical magnet. If the cylindrical magnet is placed on a material whose permeability is greater than 1, there is a minute displacement of the magnetic zero of the cylindrical magnet towards the material on which the magnet has been placed. In the lower permeability ranges, this dis-placement is a measure of the permeability of the material.

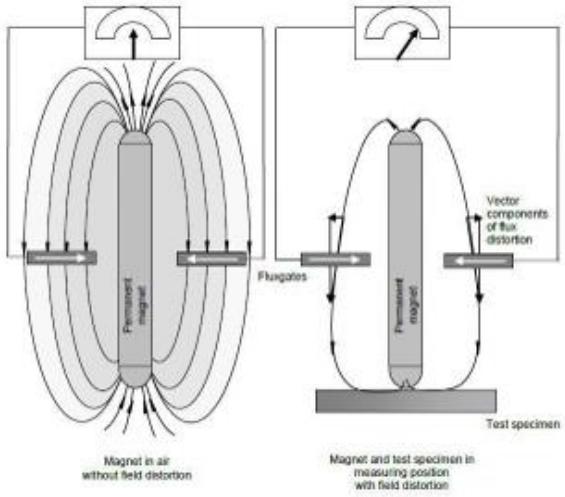

FIGURE 2.3: Schematic of the flux distortion meter arrangement and magnetic field distribution without (a) and with (b) test specimen.

Adapted from [73]
In this method, a small volume of the specimen is subjected to a local magnetic field that varies in magnitude and direction, so it is not possible to specify the magnetic field strength at which the measurement is made. The field strength at the permeability probe tip is approximately 75 kA/m.

Materials to be measured with permeability probes should be thicker than ap-proximately 8 mm whenever possible. Accurate measurements of materials that are thinner than 8 mm may be possible by stacking two pieces, but the air gap between the two pieces must be as small as possible.

The flat area on which the permeability probe is placed must not be less than ap-proximately 20 mm in diameter. When testing on curved surfaces the radius of curvature must not be less than approximately 40 mm. If any of the required di-mensions are less than those specified, the instrument will indicate permeability below the actual value [73].

At CERN, this instrument represents the standard to measure weakly magnetic materials at room temperatures.

Vibrating sample magnetometry - Test method V
In the literature, the most common method to characterize weak magnetic ma-terials is the vibrating sample magnetometer (VSM) [54], [89], [102]. A classical VSM arrangement is presented in Fig. 2.4.

Characterization of magnetic materials

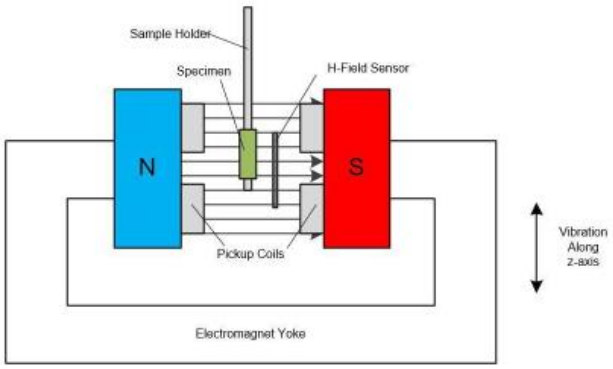

FIGURE 2.4: Schematic of a classical VSM arrangement. Adapted from [18].

The principle involved is the oscillation of a sample in a steady field, thereby in-ducing an alternating voltage in a pickup coil. This voltage is then amplified and measured by a voltmeter. For a routine laboratory magnetometer, the simplest geometry is to have the direction of the sample vibration parallel to the axes of the pickup coil and applied magnetic field [89].

Although VSM techniques are the most sensitive, their use is limited to special-ized laboratories and they are not practical from an industrial point of view, such as for a series production, due to high costs and tight constraints on the speci-men shape and volume. In [112], for instance, the thickness of the samples was 200-300 nm, and the lateral dimension 5 x 5 mm2

.

Inverse problem formulation

In recent years several works have focused their attention on inverse algorithms for the identification of the magnetic material characteristics [2], [49], [59], and [92].

In [2], the use of the electromagnetic inverse problem for the identification of magnetic material characteristic is reviewed. The inverse algorithm is combined with a generic stochastic uncertainty analysis for error estimation and reduction. The methodology is applied to characterize a commercial asynchronous machine magnetically. The case study shows good agreement between numerical and ex-perimental results, validating the proposed inverse approach.

In [49], a new approach for the characterization of magnetic materials involved in electrothermal processes is presented. In this case, the inverse analysis tech-niques are coupled with an induction heating finite-element model. In particular, the magnetic permeability is identified as a function of temperature and internal magnetic field strength.

In [59], the authors present an approach based on the use of finite element analy-sis combined with a supervised feed-forward neural network. The idea is to use the finite element method to simulate a large number of parameters in a material under test, then use this data for the training of the neural network. Finally, new materials are evaluated by the neural network obtained. The results presented in this paper prove the efficiency of the proposed approach, and encourage future works on this subject.

3. Measurement of magnetic axis displacements

Axially-symmetric magnets

In the last decades, resistive and superconductive axially-symmetric magnets have been investigated and employed at an increasing rate in several and het-erogeneous research fields [121]. As an example, in particle accelerators, mag-netic elements such as solenoids are applied in low-energy beam transport sec-tions [15], and in modern radio-frequency (RF) linear accelerators (linacs), for emittance compensation, transverse focusing, and electron cooling. Examples of resistive solenoids employed as focusing lenses in RF linacs are Linac3 [36] and Linac4 [9] at CERN. Superconductive focusing solenoids are also adopted for the project High Intense Neutrino Source (HINS) at Fermilab and the High Intensity and Energy (HIE) upgrade of the ISOLDE facility at CERN [77]. The advantage of using short solenoidal lenses in high-power accelerators, instead of sequential pairs of quadrupoles, is the reduction of the emittance growth and the related particle losses [105]. However, the application of axially-symmetric magnets goes beyond the particle accelerator research. For instance, a low-field, large-bore High Temperature Superconductive solenoid for emittance compensa-tion was designed for the superconducting radiofrequency electron gun for the WiFEL at the University of Wisconsin [26]. Magnets of this type have also been employed in many different devices, such as electron microscopes [140], particle therapy, and short-pulse radiographic diagnostics [68].

An axially-symmetric magnet is based on one or a series of axially-centered coils, producing a region of cylindrically-symmetric, radial, and axial magnetic fields. The solenoid field consists of two components: a dominant, axial component, with a maximum strength at the center of the solenoid, and a weak, radial com-ponent with relevant effects only towards the ends of the solenoid. Charged par-ticles moving outside the magnetic axis are azimuthally accelerated by the radial field component, especially in the magnet's end regions. This leads to the heli-cal motion of the charged particles in the longitudinal field region of the magnet.

Therefore, particle beams require a strict determination of the magnetic axis. In specific accelerator designs, a multi-coils solenoid could be preferred to a se-ries of solenoids, or one bigger solenoid, as focusing element for particle beams or transport, for several reasons. Multi-coil solenoids with coaxial coils were stud-ied for producing a uniform magnetic field [21, 107], or particular field configura-tions, e.g., a near-linear gradient axial magnetic field [111]. Furthermore, the use of multi-coil solenoids as focusing structures is of great interest, too. An example is the 8-GeV proton driver linear accelerator, proposed at Fermi National Acceler-ator Laboratory (FNAL), where superconducting solenoids have been employed in the front-end focusing system of the High Intensity Neutrino Source (HINS) [106, 8]. In all these cases, the alignment of the coils axes is essential for the sys-tem performance or even functionality.

Measurement methods

Axially-symmetric magnets are hardly compatible with the standard instrumen-tation optimized for accelerator multi-pole magnets and are routinely tested with expensive and time-consuming mapping systems [108]. Recently, several meth-ods have been developed to measure the magnetic field of axially-symmetric magnets and overcome the use of mappers. For instance, a novel method exploit-ing the inherent axial symmetry of the magnetic field was proposed. The method in [15, 12] is based on an induction transducer, sensitive to the longitudinal and radial components of the solenoid under test, moving along the magnet axis. The voltage induced in the transducer is then acquired and integrated digitally in or-der to yield the flux linkage as a function of the linear position, measured by a laser interferometer.

In the literature, the methods to align solenoids can be grouped in three main categories: (i) the single stretched-wire methods [44, 45], (ii) the vibrating-wire methods [14, 11, 138] and (iii) the Hall transducer-based methods [80, 109]. The single-stretched-wire method exploits the Faraday induction law: when a single conducting wire is moved inside a magnetic field, the integrated voltage across its connection terminals is a measurement of the magnetic flux linked with the surface traced out by the wire. The axis is obtained by iterating horizontal and vertical sweeps of the wire until symmetric start and end points, where the flux is null, are found. This is a standard method for finding quadrupole magnets'magnetic axes; however, in the case of solenoids, this method has a much lower sensitivity, because the intercepted transversal field components are significant only at the magnet's ends.

The vibrating-wire method, instead, is based on the Lorentz force. When a cur-rent pulse is driven through the wire, its interaction with the magnetic field gen-erates mechanical vibrations, which can be measured and put in relation with the surrounding field. This method is a standard to measure magnetic axis position in quadrupole magnets for particle accelerators. The basic idea is to find the wire position in the magnet aperture where the smallest oscillations at first and second resonance frequencies are observed [11].

This same principle was applied to solenoids [14]. When the wire position coin-cides with the magnetic axis, the transversal field components cancel out and no motion is induced on the wire. Two wire resonance frequencies are excited for co-and counter-directional movements of the wire stages in the process of center-ing and aligning a solenoid. This procedure of finding the minimum oscillation amplitudes has a sensitivity to the misalignment in the order of the micrometer. The main drawback of this method is that the procedure is applicable only if the whole solenoid's aperture is accessible. Hence, these methods cannot be applied to real-time monitoring of an operational solenoid.

A different approach for estimating the magnetic axis consists of using Hall trans-ducers. For example, the field generated by the rotation of a Hall transducer at several points along the axis of a solenoid can be recorded as a function of the ro-tation angle [80]. Then, the displacement of the axis of rotation from the magnetic axis is retrieved post-processing the solenoid field. A common way to determine the magnetic axis using Hall transducers to calculate the magnetic center is by measuring the 2D field profile of the solenoid at different positions along the z-axis and then estimating the magnetic axis position with a resolution of 0.01 mm [109]. In this case, the axial component of the magnetic field is measured, rather than the radial component. The drawback of the Hall transducer-based methods is the mapping of the full solenoid aperture, generally performed with moving stages through sturdy mechanics.

When a magnet is in operation, its coil is continuously subjected to an electrody-namic strain. This could quickly bring to a significant misalignment of the mag-netic axis from the geometric axis. In the case of a multi-coil solenoid, this effect would be even more dramatic, because the different coils could show different misalignments. Hence, a system for monitoring in real time these misalignments is essential in all applications where a strict constraint on the coils alignment is required, giving the possibility to adjust each coil position to achieve/recover the solenoid design parameters. However, the standard methods to find the mag-netic axis, introduced in this section, are not suitable for real-time monitoring, because they require that the whole solenoid's aperture be accessible.

4. Objectives of this thesis

This thesis describes the study, design and experimental activities related to the development of new methods for measuring magnetic materials and magnet axis displacements. These developments involve the following main achievements:

Revamp and upgrade of the split-coil and cryogenic permeameter. A set of new analog to digital converter (ADC), digital to analog converter (DAC) and other components have been procured, characterized and inte- grated into the measurement system. New control and post-processing soft-ware have been developed in the established C++ framework of the CERN magnetic laboratories, FFMM [16]. An extensive suite of tests has been performed in order to validate both the control and the post-processing software components. An adapted-to-low-permeability-materials approach based on a time-saving, flux-metric method has been proposed for the char- acterization of weakly magnetic materials.

Design and implementation of a superconducting permeameter. The mea-surement system is based on employing a ring sample at cryogenic temper-atures and a superconducting excitation coil. Quench protection solutions have been studied and implemented as well. The problem has arisen from the necessity to retrieve the normal magnetization curve of ARMCO®Pure Iron, the material employed as the iron yoke for the new HL-LHC magnets [115, 132].

Design and validation of a novel method for characterizing weakly mag-netic materials. The method is based on an inverse analysis approach cou-pled with a finite-element model. A material with unknown permeability is inserted into the air gap of a dipole magnet and the consequent pertur-bations of the dipole background flux density are measured and acquired in FFMM utilizing a Metrolab NMR sensor. A positioning stage, controlled by an FFMM application, allows the sensor to move around the sample and to keep track of these positions. The relative magnetic permeability is then identified through grey-box inverse modelling, based on a finite-element approach.

Design and validation of a new method for solenoid magnetic axis align-ment. A method for monitoring the coils alignment in multi-coil solenoids, directly during their operation in particle accelerators has been proposed. Few measures of the magnetic field by Hall transducers and a local field model allows monitoring the magnetic axis position of each coil, and thus, to keep a particle beam strongly focused over its operation time. The method was validated on a challenging case study on the European project “ELI Nu-clear Physics” (ELI-NP).

By employing these measurement systems, several materials have been character-ized at their operational temperature and magnetic field. In particular, the mag-netic properties of series production co-wound stainless steel tapes for quench de-tection in ITER TF coils have been measured by employing the proposed adapted-to-low-permeability-materials approach based on a flux-metric method. The mag-netic properties of the ARMCO®Pure Iron, for the construction of the supercon-ducting magnet yokes in the framework of the HL-LHC upgrade, have been mea-sured, within annealing treatment sequences from 750◦C to 850◦C, at operating temperatures of 4 K to 300 K. The dependency on the operation temperature was shown by testing the material at the cryogenic temperature of roughly 4 K, 77 K and room temperature. Finally, tests performed before and after the application of mechanical stress have also been studied to validate the production process. Another goal of this thesis has been to reduce the lack of data present in the liter-ature and to validate the use of Cryophy as the cold magnetic shield material of the crab cavities cryomodule prototype. Accurate experimental studies on sam-ples from the same heat treatment as the parts of the actual shields at CERN have been performed.

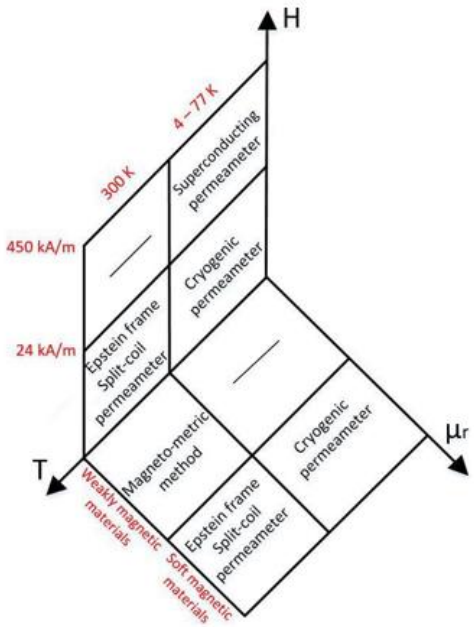

In Fig.2.5 a classification of the developed measurement systems is presented. The classification is based on: (i) maximum magnetic field, (ii) expected relative magnetic permeability and (iii) operational temperature.

The characterization of materials for magnet yokes and magnetic shielding (rel-ative permeability in the range 103-106

is performed utilizing a split-coil perme-ameter and an Epstein frame at room temperature and a cryogenic permeame-ter at cryogenic temperatures, respectively. Measurement systems, based on the flux-metric method, are explained in detail in chapter 3. In particular, the Epstein frame is used to perform the characterization in AC, at a frequency up to 400

Hz and the split-coil and cryogenic permeameters are used to perform measure-ments in quasi-static conditions. Hardware limits make it impossible to exceed an excitation magnetic field of 24 kA/m.

This limit has been exceeded by designing and employing a superconducting per-meameter. Its design, implementation and quench simulations will be described in Chapter 3. It allows measurements to be performed up to 450 kA/m in a region of the normal magnetization curve where the material is heavily saturated. The results of the characterization of ARMCO for HL-LHC at this level of saturation are presented in chapter 6.
Concerning weakly magnetic materials, an adapted-to-low-permeability-materials of the flux-metric method is used in a range of permeability among 1.1 and 6.0, whereas the results in therm of uncertainty are not satisfying when μr goes be-low 1.1. Hence, for weakly magnetic materials with a relative magnetic perme-ability μr less than 1.05, a measurement system based on a novel magneto-metric method has been developed and validated. These two measurement systems are explained in detail in chapter 4.

III. PROPOSAL FOR CHARACTERIZING SOFT MAGNETIC MATERIALS

In this chapter, the measuring principle of the flux-metric method and the en-hancements carried out in this work, concerning measurement procedure and drift correction are illustrated. Firstly, the design aspects of the experimental sup-porting technologies for data acquisition and analysis are described. Then, a so-lution for characterizing soft magnetic materials at the operational temperature of 4.2 K and a saturation level near 3 T is proposed. The measurement system employs superconducting coils. Hence, specific quench detection and magnet protection simulations are carried out. An uncertainty model and a study of re-peatability and reproducibility of the measurement procedure are presented as well.

1. The measurement principle

The experimental methods adopted in this dissertation for characterizing soft magnetic material are based on the flux-metric method described in the standard IEC 640404-4 "Magnetic materials - Part 4: Methods of measurement of d.c. mag-netic properties of iron and steel." [70].

Fig.3.1 shows a schematic representation of a standard measurement system. A sensing coil and an excitation coil are wound around the sample. The excitation coil carries the excitation current to magnetize the sample under test. This cur-rent is supplied by a current generator which is controlled by the signal provided by a digital-to-analogical converter. The sensing coil detects the induced voltage, that after integration allows the flux to be calculated and, consequently, estimate the magnetic flux density.

The magnetic field H(r, t) is evaluated from the current using

$$H(r, t) = \frac{N_e i(t)}{2\pi r} \quad (3.1)$$

where Ne is the number of turns in the excitation coil, i(t) is the imposed current and r is the distance from the center of the toroid. H is represented as a scalar for symmetry reasons.

The magnetic field is variable within the cross-sectional area of the toroid. Since

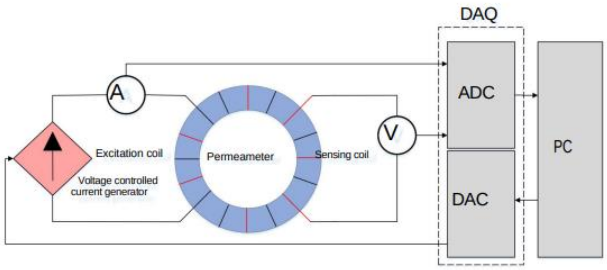

FIGURE 3.1: Architecture of the measurement system

the difference between external and internal diameter is much lower than the length of the circumference, the magnetic field is assumed constant in the cross-section and equal to its integral average between the inner and the outer radius, H0(t)

$$H_0(t) = \frac{1}{\ln\frac{r_2}{r_1}} \int_{r_1}^{r_2} \frac{S}{r} H(r, t)dr = \frac{N_e i(t)}{2\pi r_0}, \quad r_1 < r_0 < r_2 \quad (3.2)$$

After acquiring the induced voltage on the sensing coil, the magnetic flux is de-termined by integration

$$\Phi(t) = -\int_0^t v(\tau)d\tau. \quad (3.3)$$

The magnetic flux density B(t) is

$$B(t) = \frac{1}{A_s}\left(\frac{\Phi(t)}{N_s} - \mu 0 H_0(t) A_a\right) \quad (3.4)$$

where As is the cross-sectional area of the sample, Aa is the cross-sectional area of the air, as represented in Fig. 3.2.

The magnetic relative permeability is

$$\mu_r(H) = \frac{B(H)}{\mu 0 H} \quad (3.5)$$

2. Procedure and drift correction

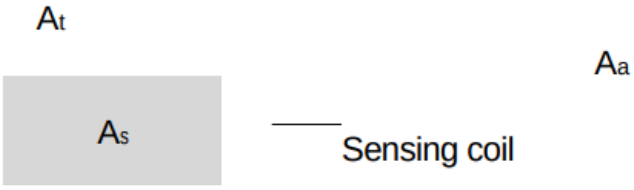

FIGURE 3.2: Representation of the cross-sectional area of the sample As and of the sensing coil Aa. The cross-sectional area of the air gap is As = At −As.

2. Procedure and drift correction

The procedure adopted for the tests, consists of three steps: i) demagnetization; ii) magnetization; and iii) post-processing.

Firstly, the sample needs to be demagnetized to remove memory-effects from the measurements. Demagnetization is performed by applying an excitation current with a decreasing exponential envelope. Magnetization is performed by ramp-ing the current back and forth between positive and negative values, with the amplitude of each plateau slightly increasing. The ramp rates and the plateau durations are selected so that dynamical effects, predominantly eddy currents, are reduced after a certain percentage of the plateau. The current during this step follows the evolution represented in Fig. 3.3.

The waveforms acquired are post-processed by applying the relations from Sec-tion 3.1, but firstly, it is necessary to correct the voltage acquisition by means of a drift correction algorithm.

The acquired voltage v(t) can be expressed as the sum of three contributions

$$v(t) = v_s(t) + v_o(t) + v_n(t) \quad (3.6)$$

where vs(t) is the zero-mean induced voltage at the terminals of the sensing coil, vn(t) is a zero-average random noise and vo(t) is the offset error, a contribution that depends on various disturbance causes. By integrating v(t)

$$\Phi(t) = \int_0^t [v_s(\tau) + v_o(\tau) + v_n(\tau)]d\tau \approx \Phi_s(t) + \Phi_o(t) \quad (3.7)$$

where Φs(t) is the magnetic flux and Φo(t) is the drift error. The contribution of the random noise is neglected because of the integration operation.

In the literature, several drift correction approaches have been proposed [55, 83, 128, 69]. The method proposed in this work can be split into the following steps:

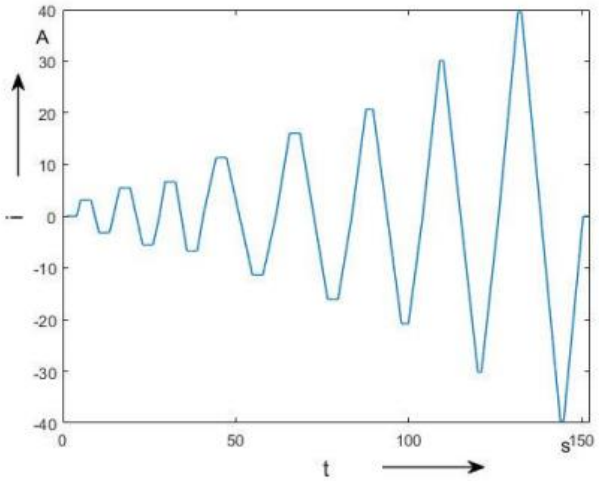

FIGURE 3.3: An example of a magnetizing current waveform

- Identify on each positive and negative plateau, the first and the last point, triangle and square symbols in Fig. 3.4.
- Estimate the point of the plateau corresponding to the end of the transient due to the ramp-up dynamic effects, circle symbol in Fig. 3.4.
- Evaluate for each plateau the offset of the sensing coil signal as the average value of the voltage between the circle and the square symbols in Fig. 3.4.
- On the ramps, the offset is estimated by linear interpolation between the offsets of the previous and successive plateau.

Fig. 3.5 and Fig. 3.6 show the estimated voltage offset and its effect on the flux, respectively.

The normal magnetization curve is evaluated by taking the points of each hys-teresis loop corresponding to the plateau after the transient. The values of the pairs (H, B) are evaluated by averaging the values on the positive and negative plateaus, excluding the points that correspond to the transients.

3. System architecture

Fig. 3.7 shows the general architecture of the proposed measurement system. The sample is magnetized employing an excitation coil, which is supplied by a voltage-controlled current generator. First, a demagnetization cycle is carried out to put the sample in a reproducible magnetic state. Then, measurements are per-formed by ramping the current between positive and negative values. Each ramp

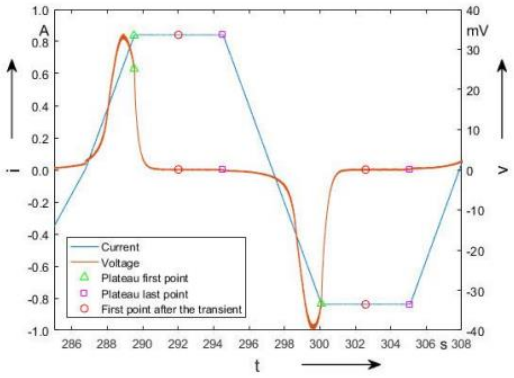

FIGURE 3.4: Normailized excitation current (light blue) and normal-ized sensing coil voltage curve (red). The triangle, circle and square symbols denote the begin of the plateau, the end of the transient phase and the end of the plateau, respectively.

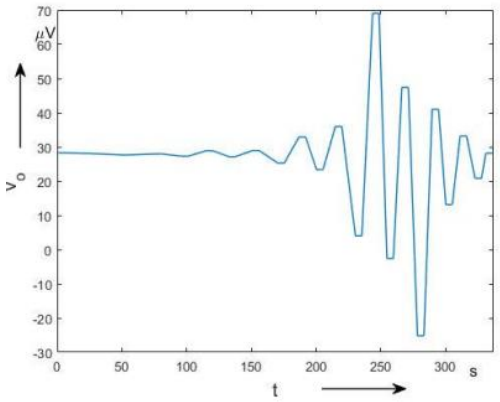

FIGURE 3.5: Example of estimated voltage offset.

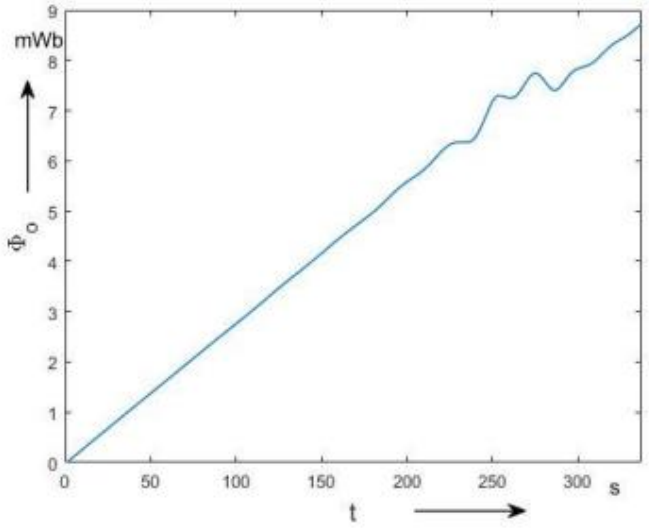

FIGURE 3.6: Flux offset corresponding to the voltage offset of Fig.3.5.

is followed by a current plateau, allowing for eddy currents to decay. Every time the current is ramped the amplitude is slightly increased to explore the initial magnetization curve progressively. During the excitation, the output voltages at both the measurement coil and the DCCT current sensor are continuously sam-pled and recorded. The voltage-controlled current generator, the digitizer, and the data acquisition board are integrated into an automatic PXI-based measure-ment station, linked to an external personal computer (PC). A suite of interactive programs, generated through the Flexible Framework for Magnetic Measurement (FFMM [10]), controls the station in order to i) calibrate both the power supply and the measuring instruments, ii) demagnetize the sample under test, iii) gen-erate the magnetizing current, iv) acquire and scale the signal in order to display the hysteresis curve, and v) measure the permeability at field values defined by the operator. In the following, the specifications of the main hardware compo-nents are described.

A voltage-controlled current generator powers the excitation coils with a current within the range ± 40 A. The current ripple must be as small as possible to avoid modulations in the DC magnetizing field and variations of the flux density along minor hysteresis loops. The current ripple and noise peak-peak is 0.5 mA on a reference load inductance of 10 mH. The power supply is also equipped with an interlock panel that sets the output to zero in case of overload/overheating. In Tab.3.1 the electrical specifications of the power supply are shown. A DCCT current transducer measures the current carried by the excitation coils with high accuracy (nearly 10−5 A), allowing correcting the

power supply's offset. The sen-sor used is a compact MACCPLUS [131], a current measuring system based on the Zero-Flux principle. The acquisition system is hosted in an Analog Device PXI crate. It consists of an ADLINK PC, an NI PXI DAQ 4461 [74] and an NI PXI DAQ series M-6289 [75], as it can be seen in Fig 3.8. The specifications of the two NI acquisition systems are shown in Tab.3.2.The two input channels of

3. System architecture

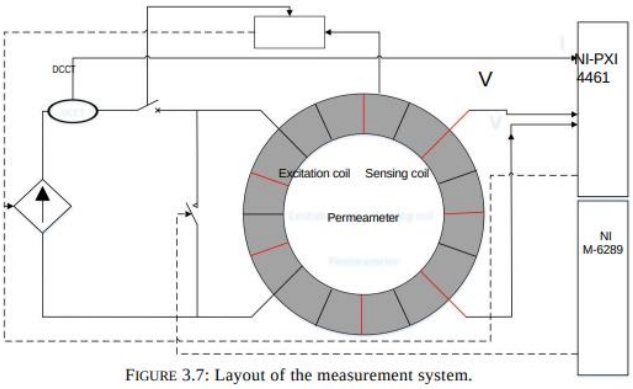

FIGURE 3.7: Layout of the measurement system.

TABLE 3.1: Power supply specifications

Parameter	Quantity
Supply voltage	*230*±23 V
Output voltage	±15 V
Non-linearity	± 0.1 %
Ripple and noise	± 0.5 mA pk-pk
Rise time	± 8 A/s
Temperature coefficient	0.2 % /K

(a) (b)

FIGURE 3.8: (a): NI DAQ series M-6289; and (b): NI DAQ 4461

the NI DAQ 4461 are used to measure the current in the excitation coil and the voltage at the terminals of the sensing coil. The high number of bits allows mea-surements to be performed with very high resolution. Another advantage is the possibility of using a very high sample rate (up to 204.8 kS/s). The NI DAQ 4461

TABLE 3.2: Specification of the NI DAQ M-6289 and 4461.

Parameters	**NI 6289**	**NI 4461** Analog input (ADC)	
resolution	18 bit	24 bit	Maximum range ± 10 V
± 42.4 V	Minimum range	± 0.1 V	± 0.316 V
Sample rate	*625 kS/s*	2014.8 *kS/s*	Analog output
(DAC) resolution	16 bit	24 bit	Maximum range
± 10 V	± 10 V	Minimum range	± 1 V ± 0.1 V

also generated the signal that controls the power supply with a high-resolution digital-to-analogical converter. A drawback is the poor stability of the first sam-ples, due to an initial transient. The adopted solution solves this problem by adding an automatic switch in parallel to the excitation coil. Switch controlled by a digital signal generated by the M-6289. During the transient, the switch is closed and it short-circuits the excitation coil. When the current is stabilized, the switch opens, the current passes through the excitation coil, and measurements can be performed. The measurements are performed by using a customized soft-ware developed in C++ and embedded in the FFMM (Flexible Framework for Magnetic Measurements) [17] framework.

Split-coil permeameter

The split-coil permeameter is an instrument conceived at CERN in the 1967 [64]. It is shown in Fig. 3.9. The split-coil permeameter consists of three toroidal coils

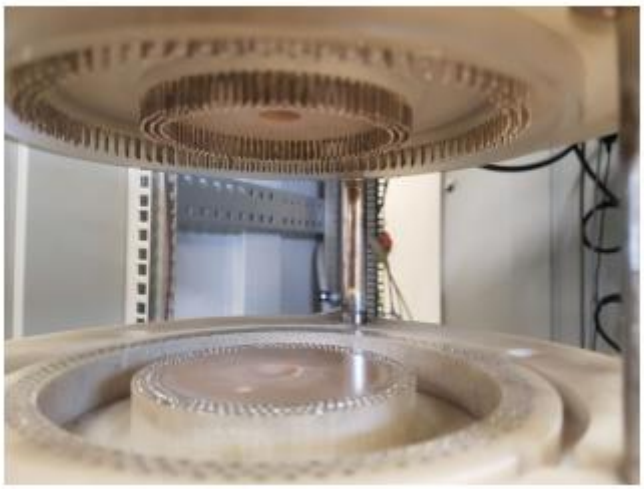

FIGURE 3.9: The split-coil permeameter.

that can be opened and closed using a customized mechanism. The design of the instrument is shown in Fig. 3.10. This system allows room temperature tests of materials' magnetic properties to be performed much faster than using a stan-dard flux-metric based measurement system. Splitting the coils into two halves has the drawback of localized heating, having two connections per turn, all in series. To curtail this problem interconnections of excellent quality have been used. The two outer coils are, generally, connected in series forming an excita-

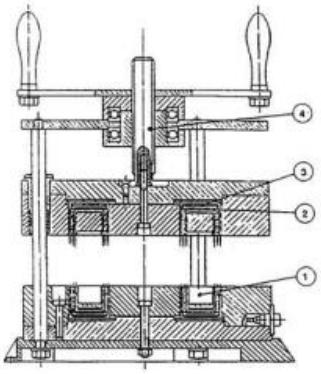

FIGURE 3.10: Section drawing of a split-coil permeameter: 1; Ring sample; 2. Sensing coil; 3. Excitation coil; 4. Opening system.

tion coil of 180 turns. With this configuration and a current of 40 A, a maximum field of 24000 A/m can be generated. The choice of the maximum current is due to a thermal limit. A circuit breaker is used to protect the instrument against overload. The circuit breaker is equipped with an auxiliary contact that moni-tors the position of the breaker. When the breaker opens, the auxiliary contact closes send a command to an interlock panel that blocks the power supply. An NTC-thermistor monitors the temperature of the coil. When the temperature of the coils is above a certain threshold, a digital signal is sent to the interlocking panel to block the power supply. The inner coil of 90 turns is, generally, adopted as sensing coil. The instrument can accommodate a ring sample up to 19.5 mm thick, having inner and outer diameters of 76 and 114 mm, respectively, and a cross-sectional area As usually derived from the geometry.

Cryogenic permeameter

The split-coil permeameter cannot be employed at the typical temperatures of the superconducting magnets for particle accelerators (T<=4.2 K). Hence, a cryogenic permeameter has been developed and installed at CERN' Cryolab test facility. The cryogenic permeameter allows magnetic characterization of materials to be performed at the cryogenic temperatures of 4.2 K in liquid helium and 77 K in liquid nitrogen. The layout of the system architecture is shown in Fig. 3.11. The measurement principle is the same as for the split-coil permeameter. At cryogenic temperature, the effect of the temperature variations can be neglected because the heat generated from the excitation coil is much lower than the cooling power of the cryogenic bath.

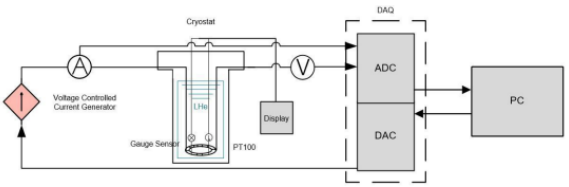

FIGURE 3.11: Layout of the Cryogenic measurement system

The sample under test needs to be manually wound with a sensing and an exci-tation coil. Generally, the sample is inserted in a case of non-thermo-shrinkable material, typically aluminum. In this way, the sample is protected from the me-chanical strain generated by the shrinkage of the coil around the sample, which may alter the sample's magnetic properties. Usually, the sample is wound with an excitation coil with 180 turns and a sensing coil of 90 turns. In the standard configuration for soft magnetic materials, the coils are made of a copper strand of 0.5 mm 2 . During a measurement, the sample and the coils are immersed in a cryogenic liquid inside a cryostat. The level of the cryogenic liquid has to be monitored because it evaporates during the process of measurement. A complete cryogenic test requires at least a working day. Fig.3.12 shows the sample prepared

FIGURE 3.12: Sample installed in the cryostat.

4. Quench protection

to be inserted in the cryostat.

Superconducting permeameter

The superconducting permeameter is an upgrade of the cryogenic permemeter based on a superconducting excitation coil. This leads to differences concern-ing sample preparation and to adopting a quench protection system. Two power diodes with a nominal current of 90 A and 600 V of nominal voltage are placed in anti-parallel for the quench protection. In Fig.3.13, a sample cross-section is shown. The sample is inserted in a case of Bluestone to prevent mechanical strain due to thermal shrink. Bluestone has been chosen among other alternatives, such as Nylon Glass Fiber, for its very low thermal coefficient (0.01% /K). In order to avoid sharp edges, the case has been designed to host a sample with a squared cross-section, but has the corners shaped as in Fig. 3.13.

Coils are wound directly on the case. The innermost layer is the sensing coil

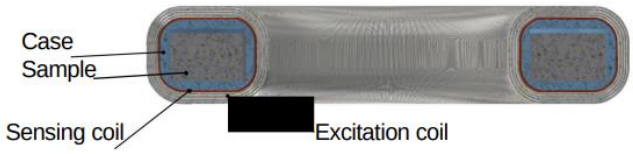

FIGURE 3.13: Sample cross-section view.

of 90 turns and 0.5 mm in diameter. The excitation coil is made of 4 layers, each one separated from the next by means of a layer of tape to prevent move-ment and mechanical disturbances. The superconducting cable used as excita-tion coil is a product of the Furukawa Electric Co., Ltd., which has the specifi-cations shown in Fig.3.14. This product has been chosen due to its low cost (1€/m), specifications regarding critical current and critical magnetic flux density and high value of insulation breakdown voltage (> 2000 V AC, Polyvinyl For-mvar). The cross-sectional diameter of the strand is 0.5 mm without insulation and 0.55 mm with insulation in Polyvinyl Formvar. The strand has a minimum residual-resistivity ratio (RRR) lower than 100 and a matrix in oxygen-free copper with a superconductor-to-copper ratio equal to 2.

The four layers of the excitation coil have respectively 566, 484, 459 and 426 turns.

A quench refers to the sudden loss of superconductivity when the coil temper-ature is raised. In the superconducting state, the resistance of the coils is zero, and hence no energy is required to maintain current flow. If the coil temperature

Type		F830/2.0/50	F830/2.0/65	F830/2.0/75	F830/2.0/85	F830/2.0/100
Superconductor		Nb-47±1wt%Ti	Nb-47±1wt%Ti	Nb-47±1wt%Ti	Nb-47±1wt%Ti	Nb-47±1wt%Ti
Bare Wire Diameter	(mm)	0.50 ± 0.01	0.65 ± 0.01	0.75 ± 0.01	0.85 ± 0.01	1.00 ± 0.01
Filaments						
- Mean Diameter (nominal)	(μm)	10.0	13.0	15.0	17.0	20.0
- Number of Filaments (nominal)		830	830	830	830	830
- Twist Pitch	(mm)	12 ± 2	15 ± 2	18 ± 2	19 ± 2	20 ± 2
- Twist Direction *1)		S	S	S	S	S
Matrix		Oxygen Free Copper	Oxygen Free Copper	Oxygen Free Copper	Oxygen Free Copper	Oxygen Free Copper
Cu to Superconductor Ratio		2.0 ± 0.2	2.0 ± 0.2	2.0 ± 0.2	2.0 ± 0.2	2.0 ± 0.2
Insulation						
- Material		Polyvinyl Formvar	Polyvinyl Formvar	Polyvinyl Formvar	Polyvinyl Formvar	Polyvinyl Formvar
- Breakdown Voltage	(Vac)	> 2,000	> 2,000	> 2,000	> 2,000	> 2,000
- Insulated Diameter	(mm)	0.55 ± 0.02	0.70 ± 0.02	0.80 ± 0.02	0.90 ± 0.02	1.05 ± 0.02
Minimum Critical Currents at 4.2K and 10^{-13}Ωm						
- Ic at 5T	(A)	> 160	> 280	> 370	> 475	> 660
- Ic at 6T	(A)	> 130	> 220	> 290	> 370	> 520
- Ic at 7T	(A)	> 100	> 170	> 220	> 280	> 400
Minimum RRR		> 100	> 100	> 100	> 100	> 100
Minimum Piece Length	(m)	5,000	5,000	3,000	3,000	3,000
Number of Piece		≦ W/50	≦ W/50	≦ W/50	≦ W/50	≦ W/50
Total weight	(kg)	W (TBD)	W (TBD)	W (TBD)	W (TBD)	W (TBD)
Length (nominal)	(m)	TBD	TBD	TBD	TBD	TBD

[Notes]
*1) Twist Direction "S" means the left hand screw twist.

FIGURE 3.14: Specifications of the superconducting strand.

rises above the superconductivity threshold, the coil suddenly develops a higher resistance. A current passing through this higher coil resistance creates heat. This heat causes a sudden, boil-off of liquid helium. A quench can occur because the field inside the magnet is too large, the rate of change of field is too large (causing eddy currents and resultant heating in the copper support matrix), or a combi-nation of the two. More rarely a defect in the magnet can cause a quench or the current density too high.

The quench protection analysis aims to assess if the intended currents for the magnet design are safe for operation. This means calculating the hotspot temper-ature of the magnet during a quench and assessing if the magnet is in need of any form of quench detection.

The protection studies consist of three cases, at the operating currents of 40 A, 80 A and 150 A, at a temperature of 4.2 K. The studies consist of several models with different tools. The first model calculates the magnetic flux density B in the magnet coil and the inductance of the coil in COMSOL. Further, a QLASA [116, 96] model was created using the magnetic flux density and inductance values from COMSOL. Lastly, the QLASA model was coupled with a PSpice circuit.

The COMSOL model is an axisymmetric 2D model of the cross-section of the toroidal coil. In the model, the cross-section of the iron sample and the Blue-stone case around the sample have the same dimensions as the real torus and case, whereas the shape of the coil is simplified. The new coil consists of a sin-gle conductor with the same current density as each winding in the original coil. The thickness of this simplified

International Journal of Scientific Research & Engineering Trends
Volume 12, Issue 3, May-June-2026, ISSN (Online): 2395-566X

conductor scales proportional to the inverse of the radius of the torus, see Fig.3.15. This scaling compensates for the fact that the winding density reduces with the radius of the torus.

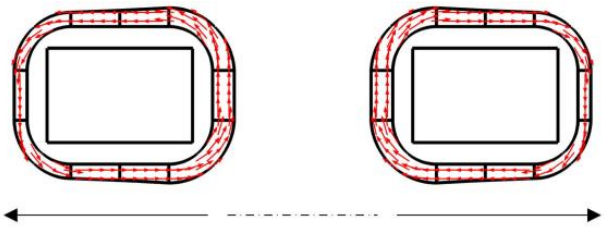

FIGURE 3.15: Current distribution used in the simulations.

From the COMSOL model, the magnetic flux density in two given points of the coil(P1 and P2) are extracted, see Fig.3.16. The points are located inside and out-side of the coil, at the smallest radius of the torus. At these points, the max value of the magnetic flux density is found. To calculate the inductance, COMSOL uses the two equations for
magnetic energy U =1 2LI2 and U =1

$$\sqrt{}_{\Omega} \boldsymbol{B} \cdot \boldsymbol{H} d\Omega, \text{ which yield}$$

$$L = \frac{1}{} \int_{\Omega} \boldsymbol{B} \cdot \boldsymbol{H} d\Omega. \qquad (3.8)$$

The magnetization curve for the iron in COMSOL is based on the curve from the MB simulations in ROXIE. The values calculated by COMSOL are shown in Table 3.3.

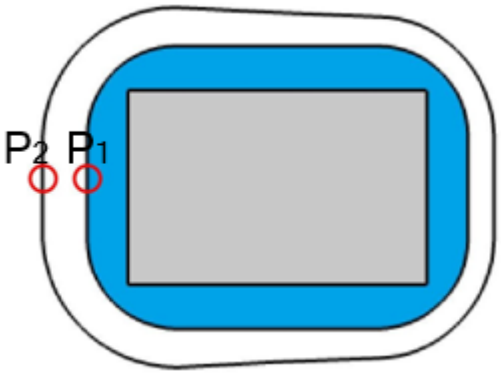

FIGURE 3.16: Cross-section of the toroidal coil with the two points, P1 and P2.

TABLE 3.3: Values of the magnetic flux density and inductance for current value.

Current I	Inductance L	$B(P_1)$	$B(P_2)$
40 A	0.04592 H	0.0040 T	0.5733 T
80 A	0.02971 H	0.0080 T	1.1466 T
150 A	0.02213 H	0.0149 T	2.1500 T

QLASA is an analytic 3D tool to calculate the quench behavior of superconduct-ing solenoids. Some assumptions were made to use QLASA on a toroidal coil and the toroidal geometry was transformed into a solenoid.

The toroidal coil is transformed into a solenoid by assuming constant cross-section and volume of the coil. The cross-section winding area of the solenoid, in Fig.3.17 (left), is approximated by the area of the innermost cross-section of the windings in the r-theta-plane of the toroidal (right). The length of the solenoid is approxi-mated to the innermost circumference of the torus with windings.

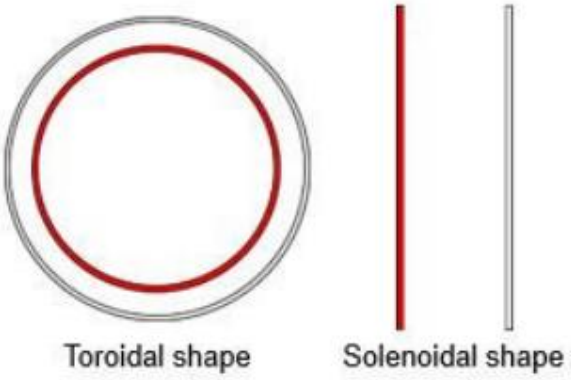

FIGURE 3.17: Cross-section area of torus in r-θ-plane and solenoid in r-z-plane. Red areas are kept constant.

The QLASA model assumes the magnetic field around the solenoid to be sym-metric with respect to the center of the solenoid. This is not the case for the toroidal coil, where the field varies with the radius of the torus. To achieve con-servative results in the simulations, the peak values of the magnetic flux density at the outside and inside of the solenoid is respectively set to P1 and P2. The magnetic flux density is assumed constant along the length of the solenoid. The QLASA simulations are based on adiabatic conditions, which implies no heat transfer to the surrounding helium.

Assuming adiabatic conditions for the toroidal coil is reasonable since the coil wires are isolated from the helium

bath, and the heating of the coil due to a quench happens in a time interval on the scale of 100 ms.

PSpice is used to simulate a circuit with the same properties as in the experimen-tal setup. The circuit setup has been simulated by adopting a power converter in parallel with the diode, represented using a switch in series with a resistance

RD equal to 1 mΩ, and the toroidal coil, represented using an inductance in se-ries with variable resistance. At nominal operation, the crowbar is open, and the power converter supplies a constant current through the coil, as shown in Fig.3.18. The crowbar is open and the current flows through the load, with r(t) equals to zero. During a superconductor quench, the resistance r(t) in the coil grows, and consequently the coil voltage increases. Once the voltage over the coil reaches a certain threshold, the power converter turns off, and the crowbar closes.

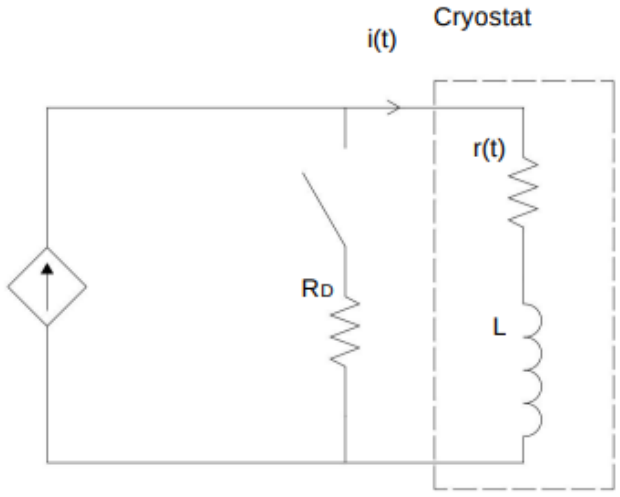

FIGURE 3.18: Electrical Circuit used for the quench protection simulations.

QLASA and PSpice are used together in the cooperative simulation framework STEAM-COSIM [28, 130, 91], where the resistance growth calculated by QLASA can be used in a custom circuit in PSpice. STEAM-COSIM is used because the in-ternal circuit setup in QLASA is not sufficient to simulate the actual circuit setup of the experiment.

In the simulations, the crowbar resistance is set to 1 mΩand the voltage threshold over the coil is set to 1 V. The results of all the operating currents for a current of 40, 80 and 150 A are shown in Fig. 3.19. From the results, the hotspot temperature rises to a maximum value of 30.4 K for 40 A, 46.5 K for 80 A and 69.7 K for 150 A, i.e., well below 100 K at which the increase in thermal expansion coefficient may result in increased stress. The results show that the toroidal coil is self-protected in all the study cases.

The threshold voltage of the power controller governs the limit of the ramp rate in the coil. The average max ramp rate is calculated from (dI/dt)max = Vt/L, where Vt is the threshold voltage and L is the inductance reported in Table 3.3. With the threshold voltage set to 1 V, the average max ramp rate is 21.7 A/s for 40 A, 33.7 A/s for 80 A and 44.2 A/s for 150 A.

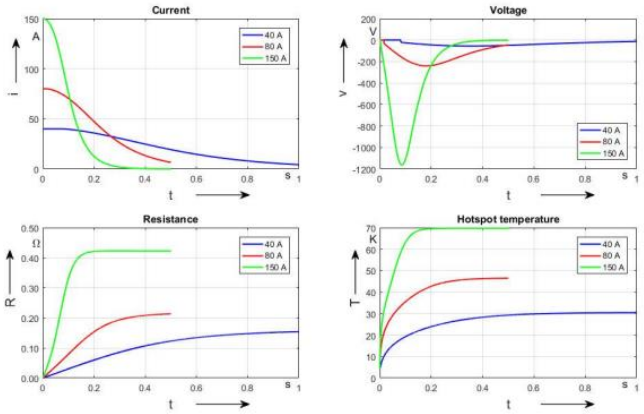

FIGURE 3.19: Current decay and hotspot temperature for three case studies.

5. Uncertainty assessment

In case of an initial magnetization curve obtained employing a point-by-point method, the IEC 60404-4 standard prescribes to adopt 2% of uncertainty on the values of the magnetic field and magnetic flux density, if current and voltage waveforms are acquired with an uncertainty lower than 1%. In this section, a more in deep the metrological performance of the proposed measurement system is presented. The used approach follows the standard Guide to the Uncertainty of the Measurement (GUM) [58]. In Fig.3.20, the architecture of the method with the measurement quantities and the main uncertainty sources is shown.

In Fig.3.21, the percentage uncertainty on the magnetic flux density, as function of the magnetic field, for a weakly (ITER Stainless steel), two soft (M140-50A and M800-100A) and a high-μ material (CRIOPHY) are shown.

The relative uncertainty always decreases as the current increases. The two steps in the soft magnetic materials' curves at 200 A/m and roughly 1500 A/m corre-sponds to a change in the gain of the ADC current channel. For magnetic fields lower

than 1000 A/m, the values of the magnetic flux density of the M140-50A are slightly higher than the values of the M800-100A. Hence, also the uncertainty curve shows the same small discrepancy at low fields. In saturation both materi-als have the same behavior, and also the relative uncertainties are equal.

For a high-permeability material, such as CRYOPHY, the uncertainty goes from 10% at low magnetic fields to 0.8% at higher fields. The high uncertainty at low fields can be justified with the number of turns of the excitation coil of the split-coil permeameter (minimum 90, maximum 180). This does not allow to generate

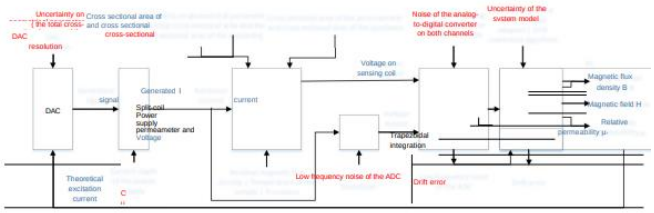

FIGURE 3.20: Architecture of the method with the measurement quantities (light blue) and the main uncertainty sources (red).

values of magnetic field small enough to be suitable for characterizing this kind of material. Another drawback of using the split-coil permeameter for such a high- μr steel is the difficulty in demagnetizing the material, with a high value of the residual flux density (about 0.2 T). This is due since the response of the mate-rial is very sensitive to external disturbances on the sensing coil's voltage. These are the reasons why the CRYOPHY for the magnetic shielding of the cryomodule of the crab cavity experiment at CERN has been tested using a customized set of 10-turns coils wound on the sample itself, details in chapter 6.

For a weakly magnetic material as the ITER stainless steel, the value of the uncer-tainty is always above 2%. This because, having the material a very low relative permeability (μr < 2), the sensing coil' signal has a lower signal-to-noise ratio. A very low sensing coil' signal means having a small flux. Hence, in Eq. 3.4 the first addend becomes smaller and the contribution of the second addend be-comes comparable with the first addend, increasing the uncertainty of the overall results. When testing stainless steel with the proposed method, the uncertainty at low fields is around 10%. The results of the magnetic characterization show that the material has a linear B-H relation.

Hence, for reducing the overall uncer-tainty of the results, the approach proposed in chapter 4 has been employed for characterizing the stainless steel of the ITER's TF coils, details in chapter 6. Fig.3.22 shows the relative expanded uncertainty on the magnetic flux densities of a soft magnetic material (M140-50A), when tested at the cryogenic tempera-ture of 4 K. For the same class of material, the results at cryogenic temperature are affected by a higher uncertainty than at room temperature. An explanation of this could be the lower voltage signal induced in the sensing coil at these temper-atures. A general recommendation for improving the measurement accuracy is to machine a sample with a thickness of, at least, 15 mm. This would also reduce the heating effect, having more volume. Another recommendation is to adopt a sample made of laminations. In order to reduce the eddy current effects, and consequently the duration of the transients, and consequently the overall time of measurement. Finally, the sampling frequency of the acquisitions should be kept

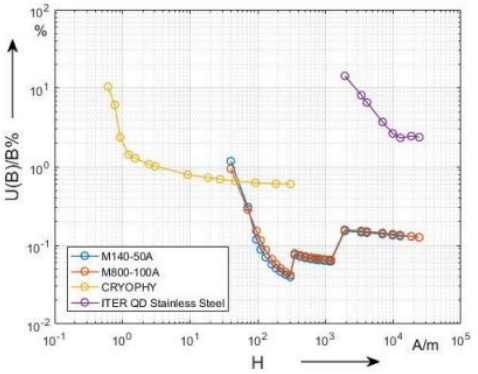

FIGURE 3.21: Expanded relative uncertainty of the magnetic flux density of several materials as function of the magnetic field. A cov-erage factor of 2 has been used.

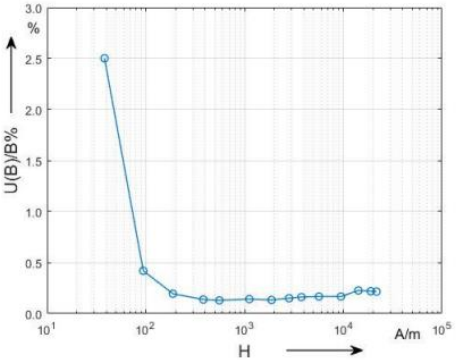

FIGURE 3.22: Relative expanded uncertainty, with a coverage factor of 2, on the cryogenic measurements of the magnetic flux densities of a soft magnetic material.

as higher as possible.

6. Conclusions

In this chapter, the problem of characterizing magnetic properties of the mag-net's yokes at their operational temperature and saturation level has been ad-dressed. The solution consists of a customized measurement system that em-ploys superconducting coils and is based on a flux-metric method. The main problem of employing superconducting coils, an undesired quench, has been ad-dressed successfully by specific quench protection simulations, which has lead to a self-protected system. An uncertainty model and a study of repeatability and reproducibility of the measurement procedure has been presented as well.

IV. PROPOSAL FOR CHARACTERIZING WEAKLY MAGNETIC MATERIALS

In this chapter, the design and validation of two methods for characterizing weakly magnetic materials, suitable to be used in the quality control of series production, are presented. An adapted-to-low-permeability-materials approach based on the previously introduced flux-metric method is proposed for characterizing mate-rial in the range of relative permeability among 1.1 and 6.0.

The results in therm of uncertainty are not satisfying when μr goes below 1.1. Hence, for materials with a relative magnetic permeability μr less than 1.05, a measurement system based on a novel magneto-metric method has been con-ceived and designed.

1. Proposed flux-metric based method

In this section, the adapted-to-low-permeability-materials approach based on the previously introduced flux-metric method is proposed for characterizing mate-rial in the range of relative permeability among 1.1 and 6.0. The method consists of applying excitation current curves with different ramp rates and measuring the respective relative permeabilities. A linear relationship between the relative permeability peak and the ramp-rates of the corresponding cycle is obtained. Consequently, by linearly fitting the relative permeability peaks values and ex-trapolating the ones corresponding to a null ramp rate, the relative permeability without the dynamic effect has been estimated.

Basic idea

The procedure is based on the assumption that eddy current effects in the sam-ple can be neglected. When the permeameter is employed for weakly magnetic materials, this hypothesis is even more reasonable. For instance, considering the case study that will be presented in this work, the typical skin depth of stainless steels is about 600 mm at the frequency corresponding to the fundamental period

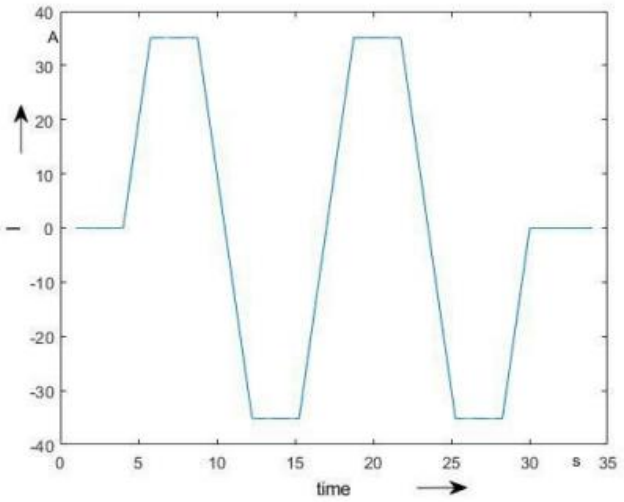

FIGURE 4.1: Example of the current driven through the excitation coil.

of the excitation, i.e. about 10 s. This assumption allows extrapolating the relative permeability curve straight from the initial magnetization curve.

To further cancel the influence of possible residual dynamic effects, the perme-ability should be measured in steady state conditions. At this aim, the excitation current has to exhibit three different cycles reaching the same maximum level on the plateau, but characterized by three different ramp-rates. As regards the max-imum current level, it has to be high enough to bring the sample in saturation; hence it depends on the material under test. For each cycle, the corresponded B-H hysteresis curve is obtained according to the classical measurement method reported in Chapter 3 and the corresponded relative permeability curve can be evaluated. From the permeability curves, then, the parameter relative permeabil-ity peak (RPP) is straightforwardly estimated. In Fig. 4.2, as an example, three RPP values, obtained for three different ramp rate values, are shown. A linear relation between the RPP and the ramp-rates of the corresponding cycle can be detected. As a consequence, by linearly fitting the RPP values and extrapolat-ing the RPP corresponding to a null ramp rate, the relative permeability without dynamic effect can be obtained.

Uncertainty source evaluation

In this section, the problems related to the use of the adapted-to-low-permeability flux-metric method for measuring the magnetic properties of weakly magnetic materials are faced.

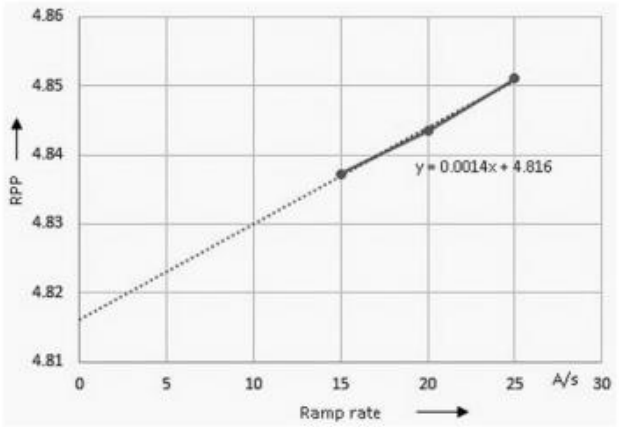

FIGURE 4.2: Relation between relative permeability estimation and ramp-rate.

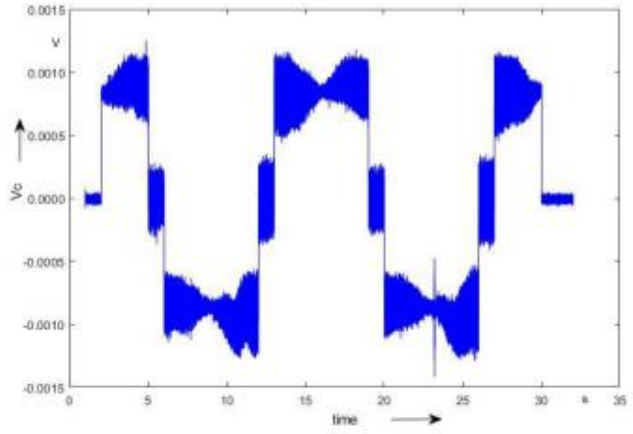

FIGURE 4.3: Example of measured voltage from the sensing coil.

Signal-to-noise ratio

The weakly magnetic materials are characterized by much lower induction val-ues if compared with high–permeability materials. As a consequence, the elec-tromotive force (emf) induced on the sensing coil of the transducer exhibits an amplitude of a few mV. An example of the signal acquired at the sensing coil is shown in Fig. 4.3. The signal is characterized by an unsatisfying signal-to-noise ratio (SNR), which could affect the overall accuracy of the permeability measure-ment. In order to enhance the performance, an analog filtering stage is required for removing the noise affecting the emf signal before its digitization.

Radial dependence of μr(H)

It is not taken into account that H(r), and hence μr(H(r)), depend upon the ra-dial position of each tape turn. The approximation made by lumping the roll at r0 is equivalent to making an average across the peak of the μr(H) curve, lead-ing thus to an underestimation of the peak permeability. The corresponding un-certainty depends upon the shape of the μr(H) curve and is often up to 2% for high-permeability steel samples.

Co-wounded tape sample

In this application, the samples are made of co-wounded tape. This leads to some considerations negligible or absent in case of bulk samples:

- The ring shape is irregular. Hence the cross-sectional area is derived from sample weight and density, instead of from geometry. This could increase uncertainty.
- The tape is very thin compared to its length. Thus the magnetization vector is expected to lie in the plane of the tape, i.e. tangent to the roll turns. This means that the in-plane component of the permeability along the tape is measured essentially, by ignoring the effects of a possible anisotropy, e.g. in the radial direction across the tape thickness.
- The tape has a spiral shape. Therefore an angle between the tape and the azimuthal H field vector arises. This angle, decreasing radially and averag-ing to roughly 0.2 mrad, causes a certain amount of flux leakage which is exacerbated by the very low permeability of the material. The small air gap between the turns represents an additional reluctance in the magnetic cir-cuit, which is not taken into account, thus leading to a slight overestimation of the material permeability.
- Additional flux leakage occurs at both the ends of the rolled tape. Some of this leakage escapes the measuring coil, while the remainder can be repre-sented as an additional reluctance in series with the magnetic circuit. As the rolls have in general more than 200 turns, the impact on the measured permeability can be expected to be of the order of the percent. However, a more detailed study would be necessary to predict whether the net effect leads to over- or underestimation of the permeability.

Drift correction

Over and above the approximations as mentioned above, the largest uncertainty sources are the meager signal-to-noise ratio and the relatively high coil volt-age offset, leading to integrator drift. As an example, the sensing coil voltage (Fig. 4.3), the

uncorrected integrated flux (Fig. 4.4), the correct integrated flux (Fig. 4.5), and the estimated voltage offset (Fig. 4.6) are reported for a standard co-wounded tape of stainless steel. The signal level is of the order of 1 mV, while the peak-to-peak noise is roughly 0.5 mV. Integration gets rid of most of the high-frequency noise, but as seen in Fig. 4.4, the measured flux is affected by a noticeable drift over the 33 s measurement duration, corresponding to a peak-to-peak offset of roughly 5 µV. The offset is not constant during the measurement

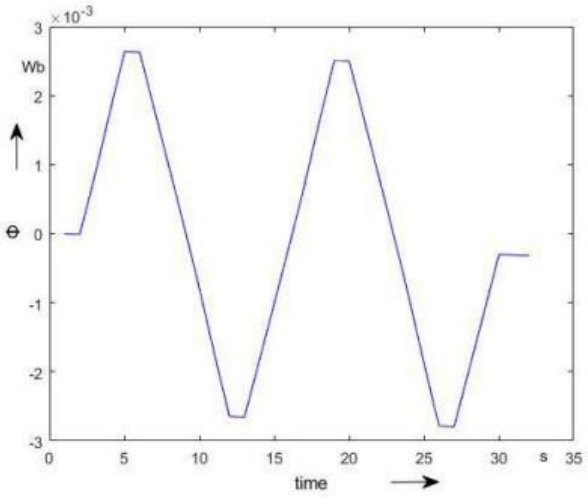

FIGURE 4.4: Uncorrected flux estimated from the sensing coil volt-age.

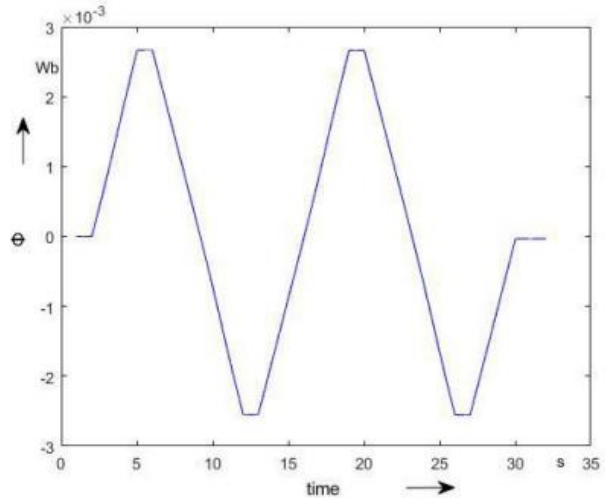

FIGURE 4.5: Flux estimated from the sensing coil voltage, drift cor-rected by means of the voltage offset estimation.

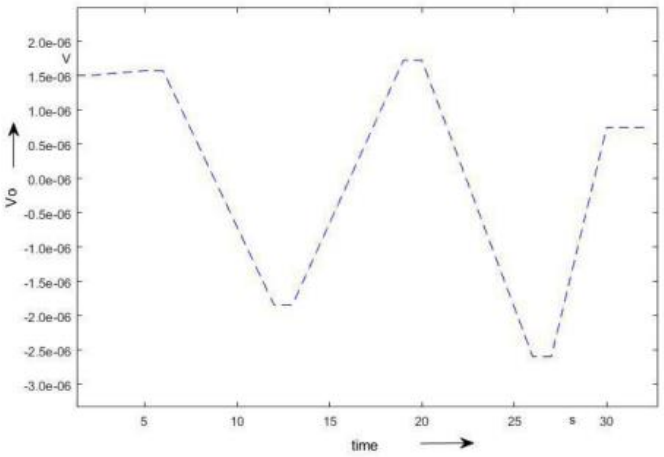

FIGURE 4.6: Measured voltage offset estimation.

and its evolution was estimated, as shown in Fig. 4.6, by making the following physics-grounded assumptions:

- the measured flux does not change between the start and the end of a cur-rent plateau. This assumption is consistent with negligible eddy current effects.
- the flux swing between current plateaux at maximum and minimum cur-rent is constant and equal to the average measured value. The symmetry of extremal magnetization states is justified by the rolls being prepared in either a demagnetized state or pre-cycled until stability is achieved before the measurement.

According to these assumptions, fluctuations of the offset of the order of ±2.5 µV are estimated during the measurement. This result is consistent with similar fixed-coil measurements in other contexts. Among the possible causes of such time-changing offset, the relatively large thermal gradients developed in the ap-paratus during the test, as well as low-frequency noise due to aliasing, may be included.

2. Proposed magneto-metric based method

The proposed flux-metric method is not suitable to test materials with a µr lower than 1.1. Hence, to face the CERN requests of testing that materials, such as IN-ERMET® IT180 for magnet radiation protection and the stainless steel for the new superconducting magnet collars, show a relative magnetic permeability peak lower than 1.005, a novel magneto-metric method has been conceived and designed.

Basic idea

The method is based on an inverse analysis approach coupled with a finite-element model. A material with unknown permeability is inserted into the air gap of a dipole magnet and the consequent perturbations of the dipole background flux

density are measured and acquired in FFMM utilizing a Metrolab NMR sen-sor [101]. A positioning stage, controlled by an FFMM application, allows the sensor to move around the sample and to keep track of these positions. The rela-tive magnetic permeability is then identified through grey-box inverse modelling, based on a finite-element approach. The 2D finite element model is realized in FEMM [100], while the inverse problem is solved in Matlab using a Levenberg-Marquardt algorithm. The schematic diagram of the measurement principle is shown in Fig. 4.7.

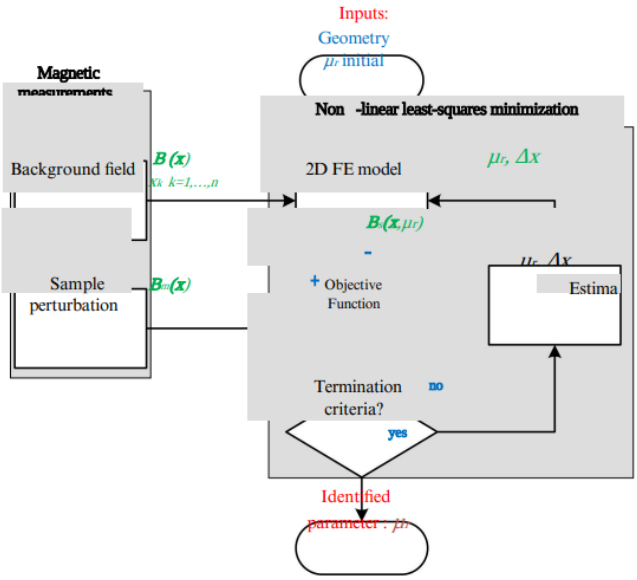

FIGURE 4.7: Flow chart of the proposed method.

Magnetic measurements
An essential part of the proposed method is to detect the perturbation of the back-ground field due to the presence of the sample under test in the dipole magnet utilizing local magnetic measurements.

Sample-induced perturbation measurements
A cylindrical sample is placed in the uniform field region of a reference dipole and the magnetic flux densities, Bm(xk), at different distances from the sample are measured with the NMR sensor. The coordinates, xk with k = 1, ..., K are measured and recorded. In this case, the problem is axisymmetric and the x axis could in principle coincide with any radius. Both the sample and the sensor are positioned symmetrically with respect to the midplane of the magnet gap.

Background field measurements
The same measurements are performed in the absence of the sample, under the same magnet excitation conditions.

Non linear least-squares minimization
The problem of the model response of physical experiments is called a forward problem, while the inverse problem theory concerns the problem of making in-ferences about a physical system starting from noisy measurements. An inverse problem is the process of calculating, from a set of observations, the causal fac-tors that produced them; it is called an inverse problem because it starts with the results and then calculates the causes.

In general, inverse problems are essentially defined as the identification problem of unknown parameters from indirect measurements. The values of the unknown model parameters are recovered by iteratively minimizing the residual between the computer forward model responses and the physical measurements.

In this application, the unknown parameter is the relative permeability of the sample under test; the physical measurements are the values of the flux density Bm(x) measured by the NMR Teslameter; and the computer forward model re-sponses are the flux density Bs(x, μr) provided by a 2D FE model of the open circuit measurement system.

Finite Element Modeling
The numerical model of the open circuit measurement system is constructed us-ing a 2-D finite element method in FEMM, using Lua as scripting language [113]. The following assumptions have been made: i) the geometry is locally 2D; ii) the permeability in the sample is uniform and iii) inserting the sample inside the magnet does not affect appreciably its total reluctance (or, in other words, the boundary conditions for the FE model correspond to a uniform field with and without the sample).

3. Conclusions
Objective Function
We have considered an objective function OF representing the quadratic error between the measured and simulated quantities:

$$[\mu^*_r, \Delta x_*] = \arg\min_{\mu_r, \Delta x} OF(\mu_r, \Delta x, \mathbf{x})$$

where μ∗ris the estimated relative magnetic permeability of the material and Δx the estimation of the distance sample-sensor offset. The first formulation (C1) is simply the quadratic sum of the relative differences between measured and simu-lated field. To improve accuracy a least squares approach has also been applied to the model, making the assumption that all variables are contaminated by noise, see Fig. 4.8. The main

sources of uncertainty are the conformity to the model as-sumptions ϵg; the flux density measurements ϵB and the position measurements, characterized by two contribution, a systematic ϵΔx and an random ϵx.

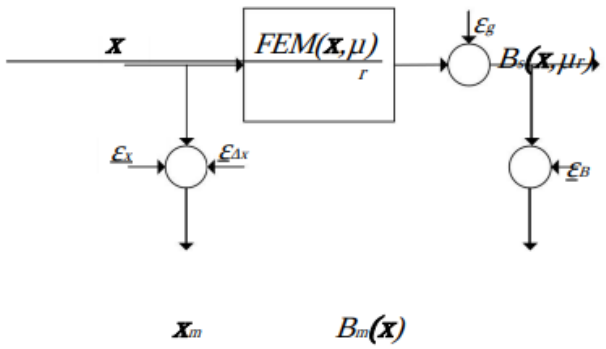

FIGURE 4.8: Diagram of the errors-in-variable approach

If the reasonable assumptions (C2) ϵg >> ϵB and ϵΔx >> ϵx are made, the objec-tive function, can be written as follows:
K

$$OF(\mu_r, \Delta x, \mathbf{x}) = \sum_{k=1}^{K} \left(\frac{B_s(x_k + \Delta x, \mu_r) - B_m(x_k)}{B_m(x_k)} \right)^2. \quad (4.2)$$

The proposed method is general and could be used with different sample ge-ometries (cube, bar, sphere) provided that appropriate 2D or 3D FE modeling is used. The main drawback is that it is not suitable for measurements at cryogenic temperature.

Conclusions

In this chapter, an approach based on a standard flux-metric method has been proposed for the characterization of weakly magnetic materials. The drawbacks related to the lack of accuracy for characterizing weakly magnetic materials due to its original conception for high permeability materials are overcome. This work can be considered as a proof of principle: the feasibility was proved and the principal uncertainty sources were pointed out and analyzed. The overall un-certainty is estimated to be less than a few percents, in repeated measurements under different drift correction assumptions.

The results in terms of uncertainty are not satisfying when μr goes below 1.1. Hence, for weakly magnetic materials with a relative magnetic permeability μr less than 1.05, a measurement system based on a novel magneto-metric method has been developed and validated. The proposed method identifies the rela-tive magnetic permeability of weakly magnetic materials immersed in a uniform, steady magnetic field. The method is general and could be used with different sample geometries (cube, bar, sphere, etc.) provided that appropriate 2D or 3D FE modeling is used.

V. PROPOSAL FOR MONITORING SOLENOIDS MAGNETIC AXIS MISALIGNMENT

In this Chapter, a novel Hall transducers-based method is proposed for the on-line monitoring of the single-coil solenoids' magnetic axis. The method relying on measurements of the magnetic flux density at a few points and a simple Tay-lor expansion as local field model. In particular, the mathematical description of the method, the involved geometrical quantities and a formulation for four trans-ducers per side are presented. However, in the presence of overlapping magnetic fields generated by several coils, the definitions of the magnetic axis and its mis-alignment, as well as the field model, are significantly more complicated. Hence, a method for monitoring the coils alignment in multi-coil magnets during opera-tions is proposed as well.

1. Proposed method for a single solenoid

Basic idea

The proposed method aims at measuring the misalignment of the magnetic axis of a solenoid by using the difference between measurements of magnetic flux density in the actual and aligned cases. The method is summed up in Fig. 5.1. The magnetic flux density is measured by two sets of Hall transducers, placed on two planes orthogonal to the nominal axis at the extremities of the solenoid.

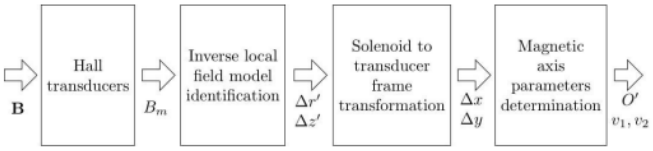

FIGURE 5.1: Main steps of the measurement method.

The measured values Bm(Hhk) at each position Hhk of the transducers are ex-ploited to identify an inverse local field model, defined by linearizing the mag-netic flux density around the positions where the transducers would move, due to the axis misalignment. The model allows to compute the displacements Δz′andΔr′of the transducer coordinates in the solenoid frame from the combination of the magnetic flux densities measured by the transducers. The displacements Δz′and Δr′are then transformed to the transducer frame and related to the Carte-sian displacements Δx, Δy of the magnetic axis interception

with the transducers planes. Finally, these displacements are used to get the parametric equation of the magnetic axis.

Mathematical formulation

The proposed method assumes that:

- From the solenoid point of view, the magnetic flux density preserves its axisymmetry even when the coil is misaligned with respect to the desired position.
- The displacements of the interceptions of the magnetic axis with the planes of the transducers are small with respect to the radial position of the trans-ducers. This assumption will be better clarified within the discussion.
- The Hall transducers are not subject to movements.
- There is no longitudinal shift for the solenoid.

For an axially-symmetric magnet, the magnetic flux density B expressed in the cylindrical coordinate system (r, ϕ, z) is independent from the angle ϕ. This means that the components of the field, namely Br, Bz, and Bϕ, are all indepen-dent of ϕ. Furthermore, for a solenoid, it is also Bϕ = 0, because B is obtained as the curl of a vector potential A = Aϕ ˆϕ, which has only a component along ˆϕ. Due to the axisymmetry, considering a circle with radius R0 centered on the solenoid axis and contained in a plane orthogonal to this same axis, the two components of B will have a constant magnitude for all the points of the circle. This implies that also the field module B is constant on such a circle.

When the solenoid is in its nominal position (aligned solenoid, Fig. 5.2a), a Carte-sian reference system with the origin at the center of the solenoid (O), and the z axis along the solenoid magnetic axis can be employed. Let us assume that eight Hall transducers are placed at the coordinates (−R0, 0), (+R0, 0), (0, −R0), (0, +R0) of the planes π1 and π2. Such planes are orthogonal to the z axis, and at positions z = ±d/2, with d the distance between them. The solenoid mag-netic axis passes through the points O1 and O2, representing the intersection of the planes π1 and π2 with the z axis. Meanwhile, the Hall transducers will be sub-jected to magnetic flux densities with the same amplitude, but with a different orientation, because they are placed at the same distance from the magnetic axis. When the solenoid is out from its nominal position (misaligned solenoid, Fig. 5.2b), the magnetic flux densities B measured by the transducers are different not only

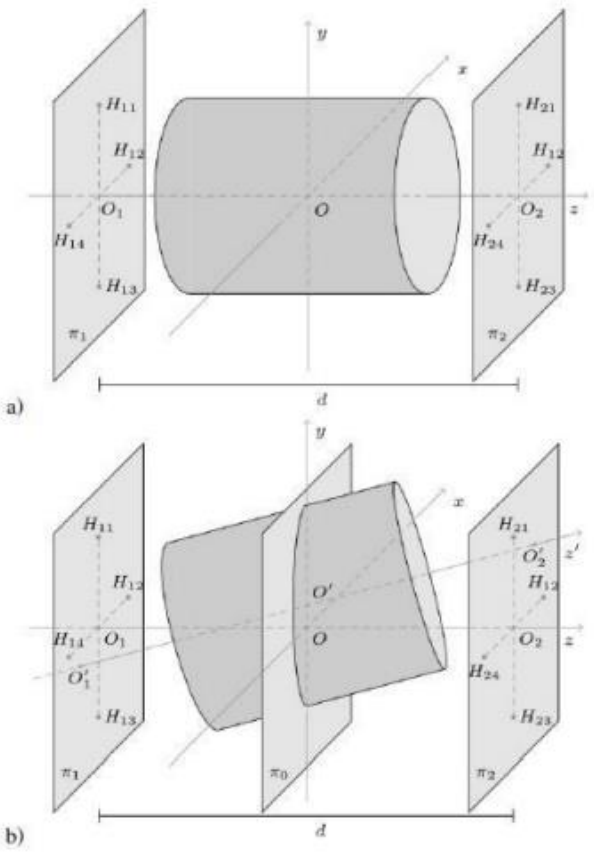

FIGURE 5.2: (a) Aligned solenoid: the magnetic axis matches with the z axis of the transducers reference system (reference axis). (b) Misaligned solenoid: the magnetic axis (z') differs from the reference axis (z), but it can be identified through O′1and O′2. in the orientation but also in the magnitude, owing to the lack of symmetry (the transducers are assumed as not subject to movements). The above-mentioned solenoid reference system is defined as a coordinate system coinciding with the transducers reference when the solenoid is aligned.

In the solenoid reference (Fig. 5.2b), the coordinates are pointed out with an apos-trophe (′), the origin is the center of the misaligned solenoid (O′), and the mag-netic axis corresponds to the z' axis. The magnetic axis is uniquely determined by the coordinates of the solenoid center O

′rameters v1, v2, v3:≡(xO′ , yO′ , zO′), and by its slope pa-

x = xO′ + v1t
y = yO′ + v2t(5.1) z = zO′ +
v3t

Indicating with O′1and O′2the intersections of the magnetic axis with the planes π1 and π2, respectively, the slope parameters are obtained as:

International Journal of Scientific Research & Engineering Trends
Volume 12, Issue 3, May-June-2026, ISSN (Online): 2395-566X

$$v1 = xo^{2-x_{O_1}}$$
$$v2 = yo^{2-y_{O_1}}$$
(5.2)
$$v3 = zo^{2-z_{O_1}}$$

Then, according to the assumption of lack of longitudinal shift, the solenoid cen-ter is constrained to the plane πo : z = 0 (Fig. 5.2b). Therefore, only radial dis-placements and tilt are considered; thus, the solenoid does not move along the z-axis. In this case, eqs. (5.1) and (5.2) are simplified as:

$$x = xo + v1t \qquad v1 = xo^{2-x_{O_1}}$$
$$y = yo + v2t \qquad (5.3)$$
$$z = d \cdot t \qquad v2 = yo^{2-y_{O_1}}$$

Local field model

According to the above assumption of small solenoid axis misalignment, the dis-tance between O1 ≡(0, 0, −d/2) and O′1and the distance between O2≡(0, 0, d/2) and O′2are small with respect to R :

$$|O^{1-O1}| = \sqrt{x_{O_1}^2 + y_{O_1}^2} \ll R_0$$
$$|O^{2-O2}| = \sqrt{x_{O_2}^2 + y_{O_2}^2} \ll R_0 \qquad (5.4)$$

Under this assumption, the field flux density is approximated with its first-order Taylor expansion around the position H′hk, corresponding to the point where the transducer would move, owing to the misalignment. Then, using such an expansion, the magnetic flux density is assessed in Hhk (the position where the trans-ducer lies). Here the subscript “h” identifies the plane where the transducer is

located (h = 1 for π1, h = 2 for π2), while “k” identifies the exact transducer of the plane.

The geometry suggests to adopt cylindrical coordinates, and, in the solenoid ref-erence system, the magnetic flux density only depends on the radial (r′) and axial (z′) coordinates, but not upon the angle (ϕ′), owing to the axisymmetry. As an example, the case of one of the transducers is highlighted in Fig. 5.3. The trans-ducer lies on the H11 position, moving to H′11owing to the misalignment. In this case, the expansion will be around the point H′11, having coordinates r′ = R0, z′= −d/2 in the solenoid reference system. In the case of a generic transducer, located at Hhk, the magnetic flux density is expanded as:

$$\mathbf{B}(r'_{hk}, z_{hk}) \approx \mathbf{B}(R0, z_h) + \frac{\partial \mathbf{B}}{\partial r}_{R0,z_h}(r'_{hk} - R0) + \frac{\partial \mathbf{B}}{\partial z}_{R0,z_h}(z'_{hk} - z_h), \qquad (5.5)$$

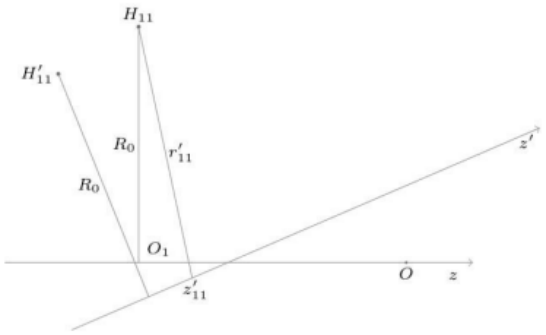

FIGURE 5.3: The position of the transducer H11 in both the trans-ducer and the solenoid reference systems. The magnetic flux density is expanded in Taylor series around the position H′11, corresponding to the point where H11 would move due to the misalignment.

where, zh = ±d/2, depending on the side of the solenoid where the transducer is placed. The first member of the equation is the quantity to be measured. In particular, uni-axial Hall transducers can be adopted, positioned along either the radial or the longitudinal direction of the transducer reference system. 1D Hall transducers placed radially are first considered.

A radial transducer measures only the radial component of B when the solenoid is aligned. Instead, when the solenoid is misaligned, also a contribution from the axial component of the field will appear. The measured value is then composed by the superposition of the projections of Br and Bz onto the radial direction of the transducer reference system. It will then depend on the magnitudes Br, Bz, and on the angles α and β, between the vectors Br and Bz and the radial direction of the transducer reference system, respectively (Fig. 5.4), again for a single transducer. The measured value is then expressed by:

$$B_m = B_{mr} + B_{mz} = B_r \cos\alpha + B_z \sin\beta \qquad (5.6)$$

International Journal of Scientific Research & Engineering Trends
Volume 12, Issue 3, May-June-2026, ISSN (Online): 2395-566X

where the projections assume negative values when directed towards the z-axis and vice versa. As an example, in the case of Fig. 5.4, Bmz has a positive value, while Bmr a negative value. Under the assumption of small misalignment, eq. (5.6) can be simplified by as-suming cos α ≈1. Then, the sign of Bmr and Br coincide. Instead, the sign of Bmz coincides with the sign of sin β because Bz is always positive. Here, Br and Bz can be expressed by Taylor expansion, as shown in (5.5). Such an expansion depends on the coordinates (r′hk, z′hk) of the transducer positions in the solenoid reference system. The derivation of the geometrical quantities as well as of sin β for the different transducers is reported in the next subsection.

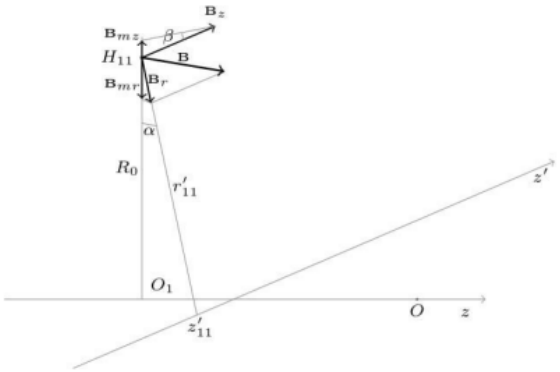

FIGURE 5.4: Br and Bz orientation with respect to the radial direc-tion on which the considered transducer is placed.

Geometrical quantities

The coordinates (r′hk, z′hk) of Hhkin the solenoid reference system (Fig. 5.5) can be expressed in terms of the points Hhk, Ihk, and O′1(or O′2), in the transducers reference. Hhk is the point where a transducer is located, Ihk its projection on the magnetic axis and O′1the intersection between the magnetic axis and the plane π1 considered in the figure.

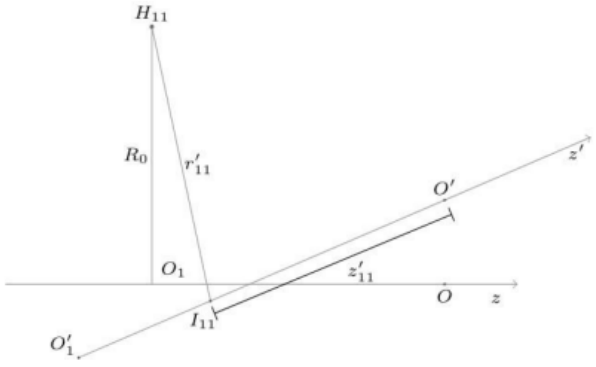

FIGURE 5.5: Coordinates (r′11, z′11) of the transducer position in the solenoid reference system.

r′hkis the distance of the transducer position from the solenoid axis, namely the distance between Hhk and Ihk ≡(xIhk , yIhk , zIhk). For example, considering H11 ≡

Proposed method for a single solenoid

(0, +R0, −d/2), eq. (5.7) holds under the hypothesis of small axis misalignment:

$$r^{11=} \sqrt{(x_{h_1})^2 + (R0 - y_{h_1})^2 + (-^{d\,2-z_{I_1}})^2 = R_0 \left(x_{h_1}\right)^2 \left(\frac{R_0}{R0 - y_{h_1}}\right)^2 + \left(\frac{R_0}{}\right)^2 + R_0 \frac{-d/2 - z_{h_1}}{R_0}^2 \approx R_0 \frac{R0 - y_{h_1}}{R_0}^2 = R0 - y_{h_1}} \quad (5.7)$$

Analogously, in the case of H13 ≡(0, −R0, −d/2):

$$r_{13}' \approx R_0 \frac{-R0 - y_{h3}}{R_0}^2 = R0 + y_{h3}$$

The points Ihk can be described with the parametrization of the magnetic axis introduced in eq. (5.3). The equation of the z′axis must be combined with the equation describing a plane orthogonal to z′and passing through the transducer Hhk ≡(xHhk , yHhk , zHhk), namely the expression (5.9).

v1(x −xHhk) + v2(y −yHhk) + d(z −zHhk) = 0 (5.9) It results that Ihk has the following parametric expression: xIhk = xO′ + tIhk v1 yIhk = yO′ + tIhk v2 zIhk = tIhk d (5.10) tIhk =v1(xHhk −xO′) + v2(yHhk −yO′) + dzHhk v2 1+ v2 2+ d2 = ≈v1(xHhk −xO′) + v2(yHhk −yO′) + dzHhk d2 z′hkis instead the distance of Ihkfrom the solenoid center. Actually, in the Taylor expansion, the term z′hk−zhis needed, and this can be obtained from the third equation of (5.10), by considering that for z1 and z2, is t = −1/2 and t = 1/2, respectively. Therefore, the following equations apply:

z′1k−z1= tI1k +1 9 d
2
(5.11)

z′2k−z2=

(t tI2k −1)
d

Basic idea

For a focusing magnet, the magnetic axis can be defined as the path where the in-tegral over the transversal field component is minimum [117]. For a single cylindrical coil, assuming that the magnetic field is axially symmetric, the magnetic axis is a straight line and coincides with the symmetry axis of the magnetic field. In particular, on the magnetic axis of the coil, the transversal field component (Br) is null [42], and the particles moving precisely along this axis are not deflected. In practice, particles must be close to the magnetic axis to be significantly fo-cused [84].

For an actual multi-coil magnet, the same definition of the magnetic axis is no longer trivial, and the equation of the magnetic axis in a proper reference frame cannot be found by applying the method proposed in the previous section. Even by assuming the magnetic field of each coil as axially symmetric, the actual mis-alignments of such fields make the overall magnetic field not axially symmetric. Therefore, in this case, the magnetic axis can be approximated with a polygonal chain, composed by as many segments as the number of the coils, where each segment is part of the magnetic axis of the corresponding coil.

Thus, by monitoring the magnetic axis, we mean deriving the polygonal chain and thus approximating the overall magnetic axis in a given reference frame. To this aim, the method for a single coil previously proposed is to be extended by relying on the axisymmetry of each coil. The basic idea is that the field measured through Hall transducers traces back to the misalignment thanks to a local field model. In particular, the model links some measurements suitably located out from the solenoid air gaps to some geometrical quantities identifying the orien-tation of the magnetic axis.

Mathematical formulation

In this section, an actual multi-coil magnet, where the magnetic fields of the dif-ferent coils are misaligned, is considered. Assuming that the magnetic field of each coil is axially-symmetric, a piecewise axial symmetry can be assumed for the magnet as a whole. Thus, the overall magnetic axis can be represented by a polygonal chain composed of the axes of each coil. In particular, excepting for the first and last coils, a segment of the axis is considered, composed by (i) half of the distance from the left adjacent coil, and half the distance from the right adjacent coil. For the first and last coils, instead, only a half line is considered, because they have only one adjacent coil. Fig. 5.6 depicts the example of a multi-coil mag-net with 4 coils, by highlighting the polygonal chain composed of the individual magnetic axes of the coils.

Such a magnetic axis can be determined by measuring the misalignment of the field of each coil, similarly to a single-coil solenoid. The assumptions underlying

V. PROPOSAL FOR MONITORING SOLENOIDS MAGNETIC AXIS MISALIGNMENT

The method are extensively treated in the previous section and are only summa-rized in the following. Regarding the field B, in a cylindrical coordinate system (r, ϕ, z), the component Bϕ is assumed as null. For the generic i-th coil, a refer-ence axis zi is considered with the origin at the aligned coil center. Two parallel planes πh and πh+1 (Fig. 5.7), with mutual distance d, are chosen at zi = −d/2 and zi = +d/2.

Hall transducers, assumed as punctiform, are placed in these planes, at the same radial distance R0 from the reference axis zi. Owing to the field symmetries, all the transducers will measure the same field magnitude, when the magnetic axis is aligned with the reference axis and different magnitudes when the magnetic axis is misaligned. The transducer locations are called Hhk, where h identifies the plane, and k the transducer within the plane. They define a Cartesian coor-dinate system xiyizi (transducers reference), where the xiyi plane is orthogonal to the zi axis. The transducers reference of each coil differs from another just for a longitudinal shift. The axis misalignment can be derived if:

- the displacements of the interceptions of the magnetic axis with the planes of the transducers are small with respect to the radial position (R0) of the transducers (small misalignment);
- the Hall transducers are not subject to movements, namely they are fiducial markers for the axis measurement (fixed transducers);
- the magnet can be subject to transverse shifts, as well as rotations, but not to longitudinal shift (longitudinally fixed magnet).

Extending the reasoning to multiple coils, a set of Hall transducers at both sides of each coil is placed. Differently from the single-coil case, however, the field mea-sured by the transducers depends also on the magnetic flux density irradiated by the other coils. The method proposed here assumes that the overall magnetic field can be modeled as the superposition of the fields of each coil. Fig. 5.7 shows the general case of one of the coils lying in the middle of the solenoid, with adja-cent transducers planes placed as briefly recalled above.

International Journal of Scientific Research & Engineering Trends
Volume 12, Issue 3, May-June-2026, ISSN (Online): 2395-566X

The parametric expression of the segment of the magnetic axis corresponding to

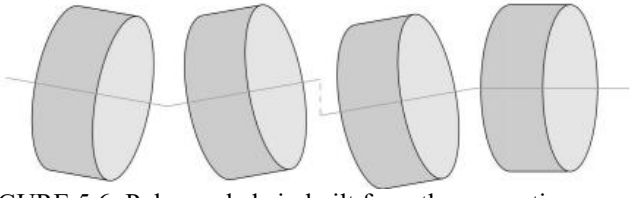

FIGURE 5.6: Polygonal chain built from the magnetic axes of coils that can move independently, but assumed as axially symmetric.

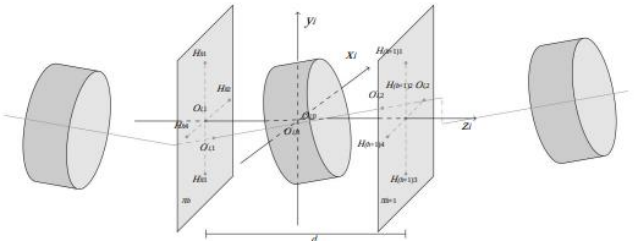

FIGURE 5.7: Hall transducers placed at the planes h and h+1 adjacent to the coil i.

$$x_i = x_{O0,i} + tv_{x,i}$$
$$y_i = y_{O0,i} + tv_{y,i} \qquad (5.23)$$
$$z_i = td$$

zi = td
is the center of the misaligned coil i, while vx,i and vy,I are the slope parameters associated to the axis. The expression of the field mea-sured by a transducer Hhk is obtained by overlapping the fields irradiated by all the N coils. If uniaxial Hall transducers are placed radially, the measured values are a combination of the radial and axial magnetic field components projections on the radial direction. When the coils misalignment is small, it results that

$$B_m(H_{hk}) \approx \sum_{i=1}^{N} [B_{r,i}(H_{hk}) + \sin \beta_{hk,i} B_{z,i}(H_{hk})]. \qquad (5.24)$$

In a generic plane h, considering the couples of transducers Hh3-Hh1 and Hh4-Hh2, respectively at x = 0 and y = 0, the expressions of interest are

$$B_m(H_{h3}) - B_m(H_{h1}) = \sum_{i=1}^{N} \{ [B_{r,i}(H_{h3}) - B_{r,i}(H_{h1})] - \frac{v_{y,i}}{d} [B_{z,i}(H_{i3}) + B_{z,i}(H_{i1})] \}$$
$$B_m(H_{h4}) - B_m(H_{h2}) = \sum_{i=1}^{N} \{ [B_{r,i}(H_{h4}) - B_{r,i}(H_{h2})] - \frac{v_{x,i}}{d} [B_{z,i}(H_{i4}) + B_{z,i}(H_{i2})] \} \qquad (5.25)$$

where the ratios between a slope parameter and d are a first-order approximation of sinβhk,i. The discussion can be conducted exclusively for the couple Hh3-Hh1, because for Hh4-Hh2 it is enough to exchange the role of yi with xi. Reasoning on the method generalization, one discovers that the expressions are to distinguish for odd and even h: in fact, an odd value for h means that a plane on the left of the considered coil is taken into account, while for even values of h the plane is on the right.

The radial and longitudinal field components in eq. (5.25) are modeled with a Taylor expansion. In particular, the method employs a first order local field model for the radial field components, as shown in eq. (5.26):

$$B_{r,i}(r_{hk}, z_{hk}) \approx B_{r,i}(R0, z_h) + \frac{\partial B_{r,i}}{\partial r}_{R0,zh} (r_{hk} - R0) + \frac{\partial B_{r,i}}{\partial z}_{R0,zh} (z_{hk} - z_h) \qquad (5.26)$$

It can be demonstrated that the only term of the Bz,i expansion that does not lead to a second-order term for vy,i in expression (5.25) is the field value at the initial point of the expansion, namely Bz(R0, zh). For each coil, the starting point for the Taylor expansion is considered in the respective transducer reference. The equations of interest are for odd h:

$$B_m(H_{h3}) - B_m(H_{h1}) = \sum_{i=1}^{N} \{ 2 \frac{\partial B_r}{\partial r} \left| e^{2\pi i(h+1-i)D} \right. y_{O0,i} + [1 \partial B_r] \left(-1 + (h+1) e^{2\pi i D} \right) \frac{\partial B_r}{\partial r} \left| e^{2\pi i(h+1-i)D} \right. d - 2R_0 \frac{\partial B_r}{\partial z} B_z \left[e^{2\pi i(h+1-i)D} \right] v_{y,i} \} \frac{d}{d \partial z} \frac{1}{1 - e^{2\pi i(h+1-i)D}} \frac{d}{} \qquad (5.27)$$

for even h:

$$B_m(H_{h3}) - B_m(H_{h1}) = \sum_{i=1}^{N} \frac{2\partial B_r}{\partial r} \Big|_{+e^{2+i\alpha 2-i\beta D}} y_{O_{0,i}}^{+} + \frac{\partial B_r}{+1 + (h - 2i^{\partial D})} + \quad (5.28)$$

where D is the distance between two adjacent coils centers when the coils are aligned. By writing the equations (5.27) and (5.28) for h = 1, 2, ..., N, and the corresponding ones for the couples of transducers (Hh4, Hh2), a linear system of 4N equations in the 4N unknowns x0,i, y0,i, vx,i, and vy,i (i = 1, 2, ..., N) is obtained. The expression for the desired quantities is too cumbersome to write explicitly, while it is easier to be solved numerically.

3. Conclusions

In this chapter, a novel method for monitoring in real time the magnetic axis mis-alignment in single-coil magnets has been presented. The method requires only a few measurements of the magnetic field at fixed positions inside the magnet aperture, and thus overcomes the main drawback of sturdy moving mechanics of other Hall sensor-based methods. Conversely to state-of-the-art axis determina-tion, the proposed method can be applied also during magnet operations, when the axis region and almost the whole remaining magnet aperture are not accessi-ble. Moreover, only a few measurements of the magnetic field at fixed positions inside the magnet aperture are required: thus a slow process such as the mapping of the whole aperture of a magnet employing moving stages is not necessary. Furthermore, a method for monitoring the coils alignment in multi-coil magnets has been proposed. This proposal extends the previous method for measuring the magnetic axis of a single-coil solenoid during its operation. In both the cases, it was shown that a set of Hall transducers and a simple first-order Taylor ex-pansion as a local field model are sufficient. In particular, for the multi-coil case, the magnetic field as a whole has been assumed as the superposition of the fields irradiated by the single coils. Simulations employing a proper field model were described to place transducers to minimize the measurement uncertainty.

In this chapter, the enhanced flux-metric method described in Chapter 3 has been employed for characterizing two materials, namely, ARMCO for magnet yokes and CRIOPHY for magnetic shields. In particular, the magnetic characterization of ARMCO®Pure Iron for the magnetic yokes of the new HL-LHC superconduct-ing dipoles and quadrupoles, is illustrated. The magnetic properties at room and cryogenic temperatures are shown, empathizing different aspects concerning the operational conditions. Moreover, a comprehensive magnetic characterization of the high- μr alloy, CRYOPHY, to be used for shielding cryogenic applications, is presented. In particular, the effects of the temperature and the mechanical strain on the magnetic properties are investigated. The attenuation test inside the mag-netic shields is, also, reported for the Crab cavity cryomodule magnetic shield prototype at CERN. Finally, the importance of magnetic material measurements in the framework of the design of magnets for particle accelerator is discussed.

Characterization of a material for magnet yoke

The construction of the superconducting magnets for the High-Luminosity up-grade of the LHC accelerator at CERN has resulted in demands for 1800 tonnes of ferromagnetic laminations for the magnet iron yokes. In this section, the mag-netic properties of the selected steel, ARMCO®Pure Iron, have been measured, within annealing treatment sequences from 750◦C to 850◦C, at operation tem-peratures of 4 K to 300 K. The dependency on the operation temperature was shown by testing the material at the cryogenic temperature of roughly 4 K, 77 K and at room temperature. Tests performed before and after the application of a mechanical stress have also been studied to validate the production process. The behavior of the material for much higher magnetic fields (8.6 to 11 T according to the field distribution in HL-LHC magnets) has been studied. Finally, the affect of the B-H curve variations on the performance of the magnets has been studied with numerical field simulations.

Validation of the proposed method for soft magnetic materials

Material and test specimen

For the production of the iron yoke laminations, the ARMCO®Pure Iron is the steel grade that better corresponds to the CERN requirements as defined in the technical specification IT4009 [132]. ARMCO®Pure Iron is low carbon steel that undergoes purification during melting by using special refining techniques. Af-ter solidification, it has a particularly homogeneous composition with regard to the impurity distribution. In the grade 4 version, ARMCO®Pure Iron presents a maximum carbon content lower than 0.003% and very low values of oxygen, sulfur, nitrogen and cobalt. Due to the low carbon content, the microstructure consists of 100% ferrite. Although, with existing technology, the carbon content has never exceeded 0.0023% with an average value of 0.0013% in the last years production.

The ARMCO®Pure Iron has a minimum Fe content of 99.85 weight%, hot rolled at 800◦C, cooled in air (not water cooled in line), with pickling and oiling of the metal sheets for rust protection. It is a non-ageing type, delivered in sheets, which are 4000 mm long and 750 mm wide. They are conditioned in 4-ton packs for the transport and storage. The sheets thickness is 5.8 mm, which is a stan-dard value for the yoke laminations used for the construction of the LHC Main Bending and Quadrupole Magnets. Due to its microstructure, the ARMCO®Pure Iron has only marginal mechanical properties. Although it was selected to match with the magnetic specification, the grade presents adequate mechanical charac-teristics (not too brittle at low temperature). For the steel sheets, CERN accepts material with a grain size ASTM lower than 6, corresponding to an ultimate ten-sile strength around 300 MPa and a yield strength around 180 MPa.

Test samples have been machined out of the coils during the sheet cutting process. In order not to alter the magnetic properties of the steel, these sam-ples have been cut at very low speed. A water jet cutting method, with abrasive powder, combined with a slow machining to obtain the required tolerances has been employed. Punching of the rings is not permitted. The samples were ob-tained as rings. The results presented here refer to the two groups of samples listed in Tab. 6.1. The former consists of 5 samples annealed as summarized in Tab. 6.1 and tested to investigate the role of annealing and cryogenic tempera-tures. The latter consists of three samples with the same annealing tested before and after the application of a cold work to investigate its role on the magnetic properties. AK steel provides the heat treatment guidelines for the annealing. In detail, the annealing parameters are: heating rate of 2-4 ◦C/min, a hold tempera-ture of 820◦C for 60 min, with an additional 15 minutes for each 0.5 cm thickness over 2.5 cm and a cooling rate of 2-4◦C/min until the parts are below 550-600◦C. The samples were tested under quasi-static conditions. The normal magnetiza-tion curve, the hysteresis loop, and the relative magnetic permeability curve have been measured utilizing the proposed flux-metric based measurement system for soft magnetic materials.

Case study I: Characterization of a material for magnet yoke

TABLE 6.1: Summary of the thermal treatment on the samples

Group #	Reference	Weight	Annealing time	Annealing time
		[g]	[◦C]	[h]
1	A	812	Not Annealed	0
1	B	815	750	1
1	C	816	750	5
1	D	816	850	1
1	E	816	850	5
2	A25112-4	256	750	1
2	A25112-3	257	750	1
2	A25114-4	256	750	1

Experimental results

Effects of the annealing on magnetic properties

The first five samples of ARMCO pure iron summarized in Tab. 6.1 have been magnetically tested at CERN to asses their magnetic properties. The tests aimed at obtaining the B-H curve for all the samples, to check (i) the magnetic properties of the material for different heating annealing, and (ii) that the magnetic proper-ties of the material are suitable for the LHC magnet construction requirements (IT4009 specification). All the samples were tested at room temperature.

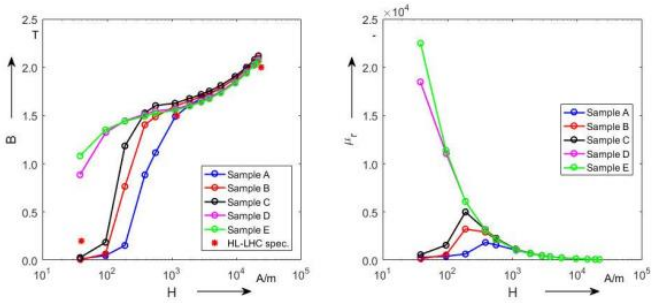

FIGURE 6.1: B-H (left) and relative permeability (right) curves for the five ring samples and the LHC specifications.

The results shown in Fig. 6.1 are from two different sets of measurements: the former for magnetic fields from 40 to 700 A/m, the latter from 700 to 22000 A/m. This is to optimize the accuracy of the obtained B-H curves, since at low fields a lower ramp rate is required. In Table 6.2, the values of the measured flux density B on the samples, at a given value of the magnetic field H, are compared with

TABLE 6.2: Summary of test results of the samples

Summary of test results of the samples

Sample	A	B	C	D	E	LHC
H [A/m]	B [T]	B [T]	B [T]	B [T]	B [T]	B [T]
40	0.01	0.01	0.03	0.89	1.08	0.20
1200	1.49	1.59	1.63	1.56	1.56	1.50
24000	2.02	2.06	2.08	2.03	2.02	2.00

LHC specifications. The initial specifications are matched by all the samples for magnetic fields higher than 1200 A/m. However, at 40 A/m only samples D and E have shown a corresponding flux density value higher than the CERN thresh-

old of 0.2 T. This is clearly a consequence of the annealing treatment at 850◦C, as increasing the annealing temperature means relaxing the residual stress. Fig 6.1 indicates the large increase of maximum permeability after the final treat-ment at 850 ◦C for 5 hours. Permeability is very sensitive to residual stresses, be-cause these impose constraints on the degrees of freedom of the domain structure, thereby engendering the rise of demagnetization fields at the grain boundaries [85]. The reasoning behind the application of an annealing process is to increase both the magnetic and the mechanical properties. Annealing influences the do-main's movement, which depends on the grain size, the micro-structure and the impurity's distribution. Furthermore, the more stressful the treatment is (high temperatures, long times of persistences at high temperatures, etc.), the higher is the influence on the magnetic properties, specially at low fields. It is noted that these differences at low fields disappear around the knee of the curve, where the magnetization rotations enter into play. Hence, in this region the effects of the annealing treatment are meaningless because the effect of the saturation's mag-netization predominant. Here, the magnetization process proceeds by rotations and the crystallographic texture remains the sole important structural property [51].

Effects of the operation temperature on magnetic properties

Since sample E has shown the highest magnetization properties, it has also been tested at cryogenic temperatures, being the right candidate to replace MAGNETIL BLTM . The aim of this test is to assess the operation performance of the material. Fig. 6.2 shows the influence of the operation temperature on the initial magneti-zation and permeability curves. Specifically, the figure displays three initial mag-netization curves at 300 K, 77 K and 4.2 K. A significant decrease of the material magnetic softening is observed when the temperature drops from 300 K to 77 K. A less significant but still appreciable decrease is observed from 77 K to 4.2 K. Cooling to cryogenic temperatures results in harder magnetic properties. This can be explained with a model of domain wall motion inhibited by inclusions. As for the annealing, it is noted that the differences observed at low fields disap-pear around the knee of the B-H curve. This means that at operation temperature the material shows a lower value of maximum relative permeability, but does not change the saturation.

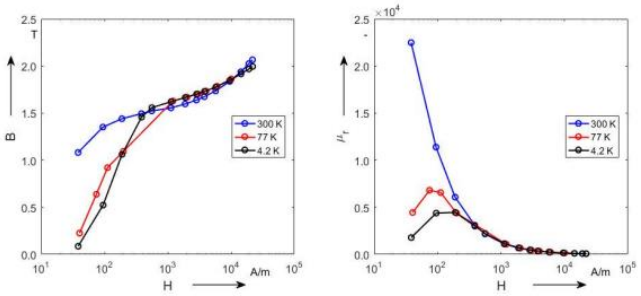

FIGURE 6.2: Initial magnetization curves and relative magnetic per-meability of sample E at 300 K, 77 K and 4.2 K

Ageing effects on the magnetic properties

After roughly three years from the first tests, a second campaign of measurements was performed on the same samples (except sample D) to verify their stability and the effects of ageing. Fig. 6.3 and Fig. 6.4 show the results of these new tests.

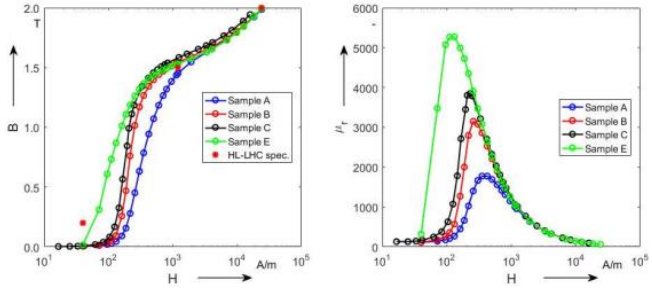

FIGURE 6.3: Results of the recent campaign measurements.

Surprisingly, sample E shows a severe degradation of its magnetic softening, spe-cially at low fields, its magnetic permeability peak going from higher than 22000 to less than 6000, while all the other samples show more or less the same mag-netic properties shown in the previous study. This behavior cannot be explained

VI. CONCLUSION

This study presented an approach for magnetic material characterization and magnet axis displacement measurement in particle accelerating systems. Accurate characterization of magnetic materials enables the determination of key magnetic properties such as magnetic field strength, permeability, and hysteresis behavior, which are essential for designing high-performance accelerator magnets. In addition, precise measurement of magnet axis displacement ensures proper alignment of accelerator components, minimizing beam

deviation and improving the overall efficiency and stability of particle acceleration.

The integration of advanced measurement techniques and data analysis methods enhances the reliability of magnet performance evaluation and alignment verification. The results demonstrate that maintaining strict control over magnetic properties and mechanical alignment is critical for achieving the required beam quality and operational accuracy in modern particle accelerators. Future work may focus on automated measurement systems, real-time monitoring, and artificial intelligence-based analysis to further improve precision, reduce maintenance time, and increase the operational reliability of accelerator facilities.

REFERENCES

1. Arpaia P, Celano B, De Vito L, Esposito A, Parrella A, Vannozzi A, Mea-suring the magnetic axis alignment during solenoids working, Nature Scientific Reports, Volume 8, Number 11426, July 2018.
2. Arpaia P, Celano B, De Vito L, Esposito A, Parrella A, Vannozzi A, On-field monitoring of the magnetic axis misalignment in multi-coils solenoids, IOP Jour-nal of Instrumentation, Volume 13, Number 8, August 2018.
3. Arpaia P, Buzio M, Liccardo A, Parrella A, Pentella M, Principe M, Ramos P, Magnetic properties of pure iron for the upgrade of the LHC superconducting dipole and quadrupole magnets, IEEE Transaction on Magnetics, published online in October 2018, doi: 10.1109/TMAG.2018.2872163.
4. Arpaia P, Buzio M, Capatina O, Langeslag S, Eiler K, Parrella A, Templeton N, Effects of temperature and mechanical strain on Ni-Fe alloy CRYOPHY for magnetic shields, Journal of Magnetism and Magnetic Materials, published online in December 2018, doi: 10.1016/j.jmmm.2018.08.055.
5. Arpaia P, Buzio M, Liccardo A, Parrella A, Pentella M, Ramos P, A super-conducting permeameter for characterizing soft magnetic materials at high fields, submitted to Journal of Magnetism and Magnetic Materials, 2018.
6. Parrella A, Arpaia P, Buzio M, Liccardo A, Ramos P, Inverse Problem-Based Magnetic Characterization of Weakly Magnetic Alloys, IPAC'17, Copenhagen, 2017.
7. Arpaia P, Celano B, De Vito L, Esposito A, Moccaldi N, Parrella A, Monitor-ing the magnetic axis misalignment in axially-symmetric magnets, IEEE I2MTC, Houston, 2018, doi: 10.1109/I2MTC.2018.8409851.
8. Eiler K, Parrella A, Arpaia P, Buzio M, Capatina O, Langeslag S, Templeton N, Characterization of Magnetic Shielding Material for HL-LHC Crab Cavities, SRF2017, Lanzhou, 2017.
9. Arpaia P, Buzio M, Liccardo A, Parrella A, On the Use of Flux-metric Meth-ods for Characterizing Feebly Magnetic Materials, IEEE I2MTC Conference Pro-ceedings, Turin, 2017, doi: 10.1109/I2MTC.2017.7969928.
10. Anglada J, Arpaia P, Buzio M, Liccardo A, Parrella A, Pentella M, Ramos P, On the importance of magnetic material characterization for the design of particle accelerator magnets, Journal of Physics Conference Series, Vol. 1065, No. 17, 2018, doi:10.1088/1742-6596/1065/5/052045.